Available online at www.sciencedirect.com
SCIENCE DIRECT®
Journal of Sound and Vibration 272 (2004) 207–243
JOURNAL OF SOUND AND VIBRATION
www.elsevier.com/locate/jsvi

Transient response and breathing behaviour of a cracked Jeffcott rotor

A.K. Darpe, K. Gupta*, A. Chawla

Department of Mechanical Engineering, Indian Institute of Technology, Hauz Khas, New Delhi110016, India

Received 23 October 2001; accepted 20 March 2003

Abstract

In this paper, a cracked Jeffcott rotor is analyzed as it passes through its critical speed and subharmonic resonances. Three different crack models are studied, namely, a breathing crack model, a switching crack model and an open crack model. The breathing crack model which closely imitates the breathing behaviour of a real crack in a rotor is studied in detail as the rotor is accelerated or decelerated past the critical speed. It is shown that the breathing behaviour and the peak response are strongly influenced by the unbalance orientation angle relative to the crack direction. The effect of acceleration rate, crack depth and damping on the breathing behaviour is analysed in this study. The effects of these parameters on breathing behaviour have not been reported earlier. Due to the accurate breathing model considered in this study, the breathing behaviour obtained is closer to reality compared to that reported in previous studies. For most values of unbalance orientation angle the breathing crack model predicts a larger response compared to the switching crack model which was used earlier in literature. The presence of higher harmonics in the response causes subharmonic resonances during coasting-up of the accelerating rotor. At these subharmonic resonances, amplitudes of the higher harmonic components have been found to be stronger in the horizontal direction than in the vertical direction. It has also been observed that during passage through these subharmonic resonances the orientation of rotor orbit changes quite noticeably. Subsequently, the peak response variation as well as orbit orientation changes have been studied experimentally. The experimental findings validate most of the analytical results. It has been experimentally observed that for an unbalance phase in the range of 67.5–135°, decelerating slotted rotor gives higher response compared to accelerating rotor. The peak response variation is typical in case of slotted and cracked rotor that can be helpful in distinguishing asymmetric rotor from cracked rotor. The orbit orientation changes during passage through subharmonic resonances are also clearly seen in experimental investigation on cracked rotors, which can prove to be a convenient tool in crack diagnosis. The experimental observations also support the analytical results of stronger horizontal component of higher harmonics near the subharmonic resonances.

*Corresponding author. Tel.: +91-11-659-1122; fax: +91-11-685-2053.
E-mail address: kgupta@mech.iitd.ernet.in (K. Gupta).

0022-460X/03/$ - see front matter
doi:10.1016/S0022-460X(03)00327-4

1. Introduction

Considerable work in the literature is available on steady state response of cracked rotors. Investigators have focused their attention mainly on two crack indicators: a 2X vibration component and a subharmonic, approximately half the shaft critical speed. The 2X vibration component is usually of small amplitude and coincides with other possible mechanisms like misalignment, looseness, coupling damage, piping forces, non-linear effects in oil film bearings, asymmetric stiffness of rotors, etc. This makes the diagnosis of crack on the basis of 2X component quite difficult and often unreliable. The second indication in the form of secondary resonance at half the shaft critical speed is detectable only for deeper cracks. Therefore the 1X and 2X vibration components characterizing steady state response have limitations in reliable prediction of crack. However many of the investigators opined that the presence of crack would be more clearly indicated during coasting-up or coasting-down than at steady state. Thus it is felt that the vibration response data during passage through the critical speed and through subcritical resonances will be valuable for general understanding of the dynamic behaviour of a cracked rotor and for reliable prediction of the same. Relatively less work is reported in literature in this direction.

Wang et al. [1], Bently and Thomson [2] have suggested that it is easier to detect cracks during start-up or run-down process than at steady speed. Nilsson [3] and Sanderson [4] presented analysis of the on-line measurement of cracked turbogenerator rotors during passage through the critical speed. Investigations on the response of a cracked rotor passing through critical speed [5–7] and also through subcritical resonances [8–10] have been carried out. Henry and Okah-Avae [11] compared response of cracked rotor with asymmetric rotor. Response of a massless shaft accelerating through its critical speed has been analyzed by Jiang et al. [12]. Sekhar and Prabhu [13] showed that oscillations in rotor response near the critical speed and the presence of subharmonic resonances are important crack indicators. Kavarana and Kirk [14] carried out an extensive experimental work on response variation with phase of unbalance for cracked rotors passing through second critical speed. Plaut et al. [15] studied behaviour of a cracked rotating shaft during passage through critical speed. They compared the response of cracked rotor using open and switching crack models.

When the rotor passes through the critical speed zone, the crack cannot be assumed to breathe the way it does at steady state operating speed away from the critical speed. Modelling the crack using sinusoidal or stepwise stiffness variation in one cycle of rotation as is done in some of the previous analyses will yield approximate results. Dimarogonas [16] emphasized the need of further study on closing crack. In this regard lately Bachschmid et al. [17] have considered breathing mechanism due to weight and thermal stresses acting on the cracked shafts. But they have considered only static bending moment. However vibrations will have considerable influence near the critical speed.

In this paper, the behaviour of a cracked Jeffcott rotor while passing through the critical speed and while passing through the subcritical resonances is studied. A breathing crack model as suggested by Jun et al. [18] is considered. They used the breathing model to study steady state response at half the shaft critical speed and observed that both switching and breathing models yielded close results. However, it is felt that the breathing model is more appropriate to correctly model the state of crack in case of transient response through the critical speed. This is because

near the critical speed, vibration amplitude is appreciable compared to that at steady operating speed away from the resonance region. The transient response of cracked rotors using the breathing model with partial crack closing has not yet been considered in the literature. The emphasis here is on studying the breathing behaviour of a cracked rotor while passing through critical speed and to study effect of various parameters on this breathing behaviour. Except a study by Plaut et al. [15], no other work could be found in literature that deals with this aspect. They considered very high order of acceleration rates that are not encountered in practice. At such high acceleration rates, the breathing behaviour obtained is bound to be different than at normal rates of acceleration. The effect of acceleration rate, crack depth, damping and unbalance phase relative to crack on the breathing behaviour is studied. Most of these parameters also influence peak response variation. Similarly most of the previous studies on passage through subharmonic resonances discussed time domain and frequency content of the signal at these speeds. In the present study, the orbit plots near subharmonic resonances are also studied to probe the effect of phase change across the fractional critical speeds on the orbit orientation.

A simple Jeffcott rotor with a transverse crack at the centre of the span is considered. Three crack models are investigated. The first, which we will refer to as breathing crack model, allows for partial opening and closing of the crack. The second model, called switching crack model, allows the crack to remain either fully open or fully closed. The last model considered is the open crack model in which the assumption is that the crack always remains fully open all the time. Results of transient response for all the three models are compared. The breathing crack model which permits modelling of partial opening/closing of crack is obviously the most refined crack model, the results from which are expected to give better insight into the transient rotor behaviour.

2. Equations of motion and crack models

Consider a massless elastic shaft of diameter D and length L with a disk of mass m mounted at mid-span. The transverse crack at the centre of span has a depth a. The co-ordinates y, z and ξ, η represent the stationary and rotating axes respectively as shown in Fig. 1a. The eccentricity of the centre of the disk mass from the geometric centre of the disk is ε and β represents the orientation of the eccentricity in the direction of the shaft rotation from the ξ axis. $\theta(t)$ is the instantaneous angle of rotation. The damping coefficient is c.

2.1. Breathing crack model

Considering direct stiffnesses k_ξ, k_η and cross coupled stiffnesses $k_{\xi\eta}$ and $k_{\eta\xi}$ which come into act due to partial opening of the crack, the equations of motion including angular acceleration terms can be expressed in the rotating co-ordinates as [18,19]

$$\begin{aligned} m(\ddot{\xi} - 2\dot{\theta}\dot{\eta} - \dot{\theta}^2\xi) + c(\dot{\xi} - \dot{\theta}\eta) + k_\xi\xi + k_{\xi\eta}\eta &= m\varepsilon\dot{\theta}^2\cos\beta - mg\cos\theta + m\varepsilon\ddot{\theta}\sin\beta, \\ m(\ddot{\eta} + 2\dot{\theta}\dot{\xi} - \dot{\theta}^2\eta) + c(\dot{\eta} + \dot{\theta}\xi) + k_{\eta\xi}\xi + k_\eta\eta &= m\varepsilon\dot{\theta}^2\sin\beta + mg\sin\theta - m\varepsilon\ddot{\theta}\cos\beta. \end{aligned} \quad (1)$$

Stiffnesses in the equations of motion are response dependent causing the equations to be non-linear. The stiffness depends on the amount of crack opening and the same can be estimated from

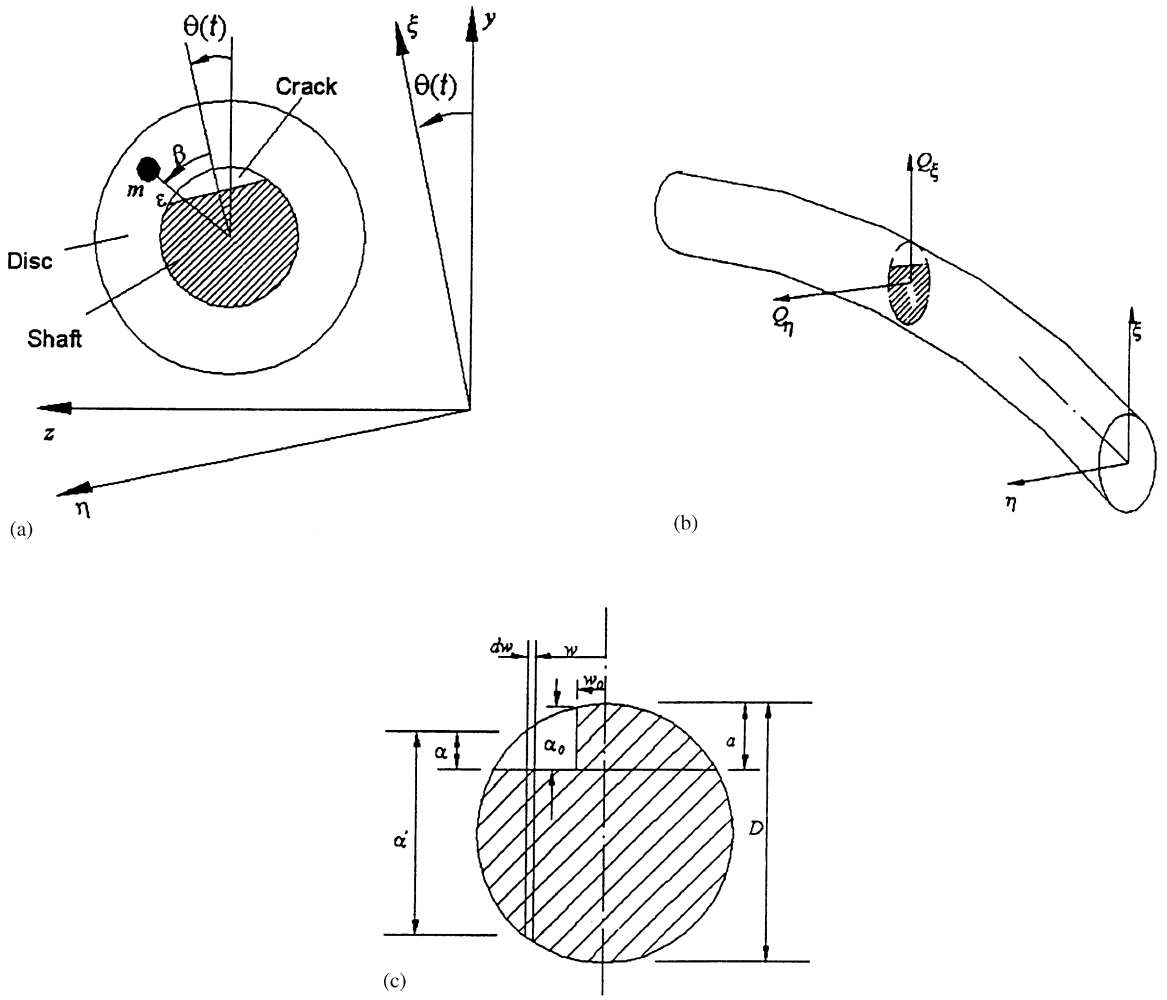

Fig. 1. Details of the cracked rotor. (a) Co-ordinate system, (b) forces acting on the cross-section containing the crack, (c) details of the crack cross-section geometry [18].

the stress field along the crack tip. Negative stress intensity factor (SIF) indicates compressive stress field and the crack is closed at that point along the crack tip, whereas a positive SIF indicates tensile stress field and the crack in an open state. The SIF is estimated with the assumption of pure bending and no shear deformation. The breathing crack model uses sign of SIF along the crack edge to decide the amount of closure of crack and thereby estimates the stiffness values to be used in the equations of motion.

Referring to Fig. 1b, the forces Q_ξ and Q_η acting on the shaft contribute together to the total stress field along the crack edge. The stress intensity factor, which is indicative of the magnitude of this stress field, varies along the crack edge and hence is a function of w (Fig. 1c). The total stress intensity factor K^I [18,20] is expressed as follows

$$K^I = K^I_{Q_\xi} + K^I_{Q_\eta}. \tag{2}$$

Here,

$$K_{Q_\xi}^I = \sigma_\xi \sqrt{\pi\alpha} F(\alpha/\alpha'),$$
$$K_{Q_\eta}^I = \sigma_\eta \sqrt{\pi\alpha} F'(\alpha/\alpha'), \tag{3}$$

are the SIF due to Q_ξ and Q_η respectively. Here σ_ξ and σ_η are the bending stresses due to Q_ξ and Q_η respectively. These are given by

$$\sigma_\xi(w) = \frac{(Q_\xi L/4)\alpha'/2}{I}, \quad \sigma_\eta(w) = \frac{(Q_\eta L/4)w}{I}, \tag{4}$$

and the functions F and F' are given by

$$F(\alpha/\alpha') = \sqrt{\frac{2\alpha'}{\pi\alpha}\tan\left(\frac{\pi\alpha}{2\alpha'}\right)}\frac{0.923 + 0.199\left[1 - \sin(\pi\alpha/2\alpha')\right]^4}{\cos(\pi\alpha/2\alpha')}, \tag{5}$$

$$F'(\alpha/\alpha') = \sqrt{\frac{2\alpha'}{\pi\alpha}\tan\left(\frac{\pi\alpha}{2\alpha'}\right)}\frac{0.752 + 2.02(\alpha/\alpha') + 0.37\left[1 - \sin(\pi\alpha/2\alpha')\right]^3}{\cos(\pi\alpha/2\alpha')}, \tag{6}$$

where

$$I = \left(\frac{\pi}{64}D^4\right) \text{ and } \alpha' = \sqrt{D^2 - (2w)^2}. \tag{7}$$

The additional deflection $\hat{u}_i$, due to the crack is given by [20]

$$\hat{u}_i = \frac{\partial}{\partial Q_i}\left[\int J(\alpha)\,\mathrm{d}\alpha\right], \tag{8}$$

where the strain energy density function is given by

$$J(\alpha) = \frac{1}{E}(K_{Q_\xi}^I + K_{Q_\eta}^I)^2. \tag{9}$$

The flexibility due to crack is now defined as

$$g_i = \frac{\partial \hat{u}_i}{\partial Q_i}. \tag{10}$$

Adding flexibility of uncracked shaft to additional flexibility due to crack, we obtain following flexibility coefficients

$$g_\xi = \frac{L^3}{48EI} + \iint \frac{128L^2\alpha'^2\alpha}{E\pi D^8}F(\alpha/\alpha')^2\,\mathrm{d}\alpha\,\mathrm{d}w,$$
$$g_\eta = \frac{L^3}{48EI} + \iint \frac{512L^2w^2\alpha}{E\pi D^8}F'(\alpha/\alpha')^2\,\mathrm{d}\alpha\,\mathrm{d}w,$$
$$g_{\xi\eta} = g_{\eta\xi} = \iint \frac{256L^2\alpha' w}{E\pi D^8}\alpha F(\alpha/\alpha')F'(\alpha/\alpha')\,\mathrm{d}\alpha\,\mathrm{d}w. \tag{11}$$

Using the above flexibility values, the following stiffness values are obtained

$$k_\xi = \frac{g_\eta}{g_\xi g_\eta - g_{\xi\eta}^2}, \quad k_\eta = \frac{g_\xi}{g_\xi g_\eta - g_{\xi\eta}^2}, \quad k_{\xi\eta} = k_{\eta\xi} = \frac{-g_{\xi\eta}}{g_\xi g_\eta - g_{\xi\eta}^2}. \tag{12}$$

It should be noted that the limits of integration in the expression of flexibility coefficients mentioned above depend on the amount of crack opening [18]. This can be established from the sign of the total SIF (Eq. (2)) along the crack edge. Integration is to be performed only for the open part of the crack.

Introducing the following dimensionless parameters:

$$\bar{\xi} = \xi/\delta_{st}, \quad \bar{\eta} = \eta/\delta_{\mathrm{st}}, \quad \zeta = \frac{c}{2\sqrt{k_0 m}}, \quad \tau = \omega_0 t, \quad e = \varepsilon/\delta_{st}, \quad \Omega = \dot{\theta}/\omega_0, \quad \lambda = \ddot{\theta}/\omega_0^2,$$

$$r_\xi = \omega_\xi/\omega_0, \quad r_\eta = \omega_\eta/\omega_0, \quad r_{\xi\eta} = \omega_{\xi\eta}/\omega_0, \quad r_{\eta\xi} = \omega_{\eta\xi}/\omega_0,$$

where

$$\delta_{st} = mg/k_0, \quad \omega_0 = \sqrt{\frac{k_0}{m}}, \quad \omega_\xi = \sqrt{\frac{k_\xi}{m}}, \quad \omega_\eta = \sqrt{\frac{k_\eta}{m}}, \quad \omega_{\xi\eta} = \sqrt{\frac{k_{\xi\eta}}{m}}, \quad \omega_{\eta\xi} = \sqrt{\frac{k_{\eta\xi}}{m}}, \tag{13}$$

and k_0 is stiffness of uncracked rotor, the equations of motion (1) can be written in dimensionless form as

$$\begin{aligned} &\ddot{\bar{\xi}} + 2\zeta\dot{\bar{\xi}} - 2\Omega\dot{\bar{\eta}} + (r_\xi^2 - \Omega^2)\bar{\xi} + (r_{\xi\eta}^2 - 2\zeta\Omega)\bar{\eta} = e(\Omega^2\cos\beta + \lambda\sin\beta) - \cos\theta, \\ &\ddot{\bar{\eta}} + 2\Omega\dot{\bar{\xi}} + 2\zeta\dot{\bar{\eta}} + (r_{\eta\xi}^2 + 2\zeta\Omega)\bar{\xi} + (r_\eta^2 - \Omega^2)\bar{\eta} = e(\Omega^2\sin\beta - \lambda\cos\beta) + \sin\theta. \end{aligned} \tag{14}$$

The solution process for solving the above equations of motion is iterative and is detailed in Fig. 2. The initial displacement is assumed equal to the static deflection of the rotor and initial stiffnesses correspond to that of an uncracked rotor. Using these initial displacements and stiffnesses, the program evaluates forces (Q_ξ and Q_η) on the crack cross-section with the help of following equations:

$$\begin{aligned} Q_\xi &= k_\xi\xi + k_{\xi\eta}\eta, \\ Q_\eta &= k_{\eta\xi}\xi + k_\eta\eta. \end{aligned} \tag{15}$$

Then using these forces, SIF at 50 points across the crack edge is evaluated using Eq. (2). Positive SIF values indicates the amount of open part of the crack. This in turn decides the limits of integration for Eq. (11) since only open part of the crack is accounted for in finding the additional flexibility due to crack. The calculated flexibility values give stiffness values using Eq. (12). Then, Eq. (14) is integrated using fourth order Runge–Kutta procedure using initial assumed response and stiffness values. A program in MATLAB (version 5.3) is written to implement the solution procedure. Stiffness values are assumed to be constant for a period of 0.001 s, for which the integration of Eq. (14) is carried out with sufficiently small time step ($\Delta t = 0.00001886$ s) for accurate solution. The speed and angular position is constantly updated using the given acceleration rate. The response obtained at the end of 0.001 s is stored and again used to re-evaluate forces using Eq. (15). These forces are used to evaluate SIF and eventually the next set of stiffness values which are then used in equation of motion to get next set of displacements (ξ and η). Thus in an iterative procedure, response is used to evaluate stiffnesses which in turn give next set of response.

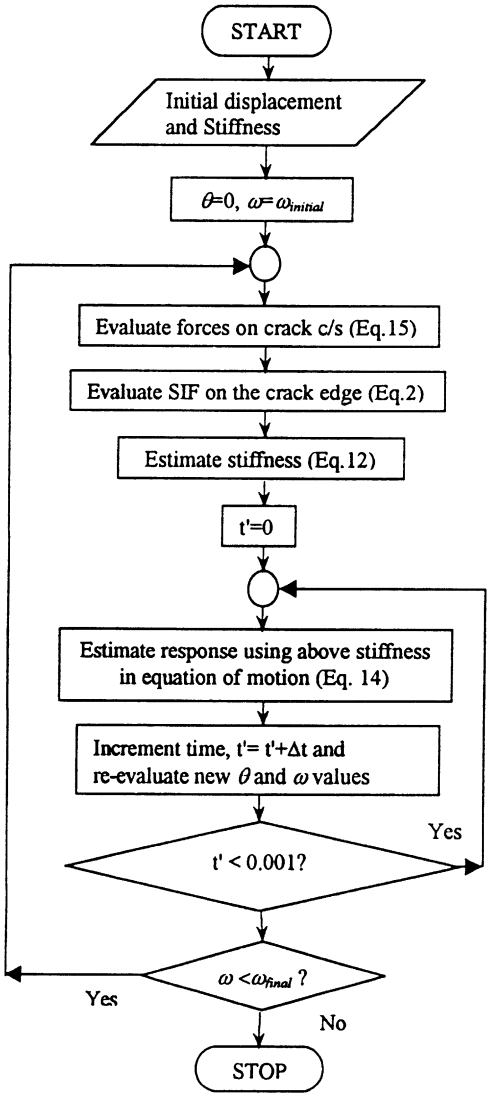

Fig. 2. Flowchart showing the procedure of solution of equations of motion.

2.2. The switching crack model

When we assume the crack to remain either fully open or fully closed, i.e., absence of partial opening or closing, the cross-coupled stiffnesses vanish and the direct stiffness possess bi-levels. The crack is now fully open or fully closed depending upon the sign of the shaft deflection in the ξ direction. The stiffnesses in ξ and η directions are equal to k_0 if ξ is negative (crack is fully closed) and equal to $\hat{k}_\xi$ and $\hat{k}_\eta$ respectively, if ξ is positive (crack is fully open). $\hat{k}_\xi$ and $\hat{k}_\eta$ are thus stiffnesses in ξ and η directions when the crack is fully open. The equations of motion (1) can now

be modified as follows [21]

$$\begin{aligned} &m(\ddot{\xi} - 2\dot{\theta}\dot{\eta} - \dot{\theta}^2\xi) + c(\dot{\xi} - \dot{\theta}\eta) + [k_0 - 1/2(k_0 - \hat{k}_\xi)(1 + sign(\xi))]\xi \\ &\quad = m\varepsilon\dot{\theta}^2 \cos\beta - mg\cos\theta + m\varepsilon\ddot{\theta}\sin\beta, \\ &m(\ddot{\eta} + 2\dot{\theta}\dot{\xi} - \dot{\theta}^2\eta) + c(\dot{\eta} + \dot{\theta}\xi) + [k_0 - 1/2(k_0 - \hat{k}_\eta)(1 + sign(\xi))]\eta \\ &\quad = m\varepsilon\dot{\theta}^2 \sin\beta + mg\sin\theta - m\varepsilon\ddot{\theta}\sin\beta. \end{aligned} \tag{16}$$

The above equations can be written in dimensionless form as

$$\begin{aligned} &\ddot{\bar{\xi}} + 2\zeta\dot{\bar{\xi}} - 2\Omega\dot{\bar{\eta}} + \{[1 - 1/2(1 - r_\xi^2)(1 + sign(\xi))] - \Omega^2\}\bar{\xi} - 2\zeta\Omega\bar{\eta} = e(\Omega^2\cos\beta + \lambda\sin\beta) - \cos\theta, \\ &\ddot{\bar{\eta}} + 2\Omega\dot{\bar{\xi}} + 2\zeta\dot{\bar{\eta}} + 2\zeta\Omega\bar{\xi} + \{[1 - 1/2(1 - r_\eta^2)(1 + sign(\xi))] - \Omega^2\}\bar{\eta} = e(\Omega^2\sin\beta - \lambda\cos\beta) + \sin\theta. \end{aligned} \tag{17}$$

2.3. The open crack model

When the crack is assumed to be open all the time, the equations are no more non-linear and are simplified to the following:

$$\begin{aligned} &\ddot{\bar{\xi}} + 2\zeta\dot{\bar{\xi}} - 2\Omega\dot{\bar{\eta}} + (r_\xi^2 - \Omega^2)\bar{\xi} - 2\zeta\Omega\bar{\eta} = e(\Omega^2\cos\beta + \lambda\sin\beta) - \cos\theta, \\ &\ddot{\bar{\eta}} + 2\Omega\dot{\bar{\xi}} + 2\zeta\dot{\bar{\eta}} + 2\zeta\Omega\bar{\xi} + (r_\eta^2 - \Omega^2)\bar{\eta} = e(\Omega^2\sin\beta - \lambda\cos\beta) + \sin\theta. \end{aligned} \tag{18}$$

3. Response during passage through first critical speed

Time domain response is computed by numerically integrating the above equations using Runge–Kutta method. Irrespective of the model used, the initial conditions for the solution of equations of motion are assumed to be those corresponding to static deflection of rotor. The rotor is initially rotating at a slow roll speed of 100 r.p.m. i.e., 10.47 rad/s ($\Omega = 0.04$) and then accelerated past rotor critical speed to 4000 r.p.m. i.e., 418.88 rad/s ($\Omega = 1.56$). The acceleration is assumed to be constant. During deceleration the rotor is initially rotating at the speed of $\Omega = 1.56$ and then decelerated to $\Omega = 0.04$. Unless otherwise specified, unbalance of $e = 0.1$ is considered in all simulations.

3.1. Breathing behaviour of accelerating and decelerating rotor

Vertical displacement is evaluated in each case after transforming results from rotating to stationary co-ordinates. Fig. 3a shows rotor response $\bar{y}$ in vertical direction versus dimensionless time τ for dimensionless acceleration of $\lambda = 0.0014$ and $\bar{a} = 0.3$. The figure also shows stiffness ratio (k_ξ/k_0) variation with respect to time τ during the passage through critical speed. The response shows maximum non-dimensional vertical rotor displacement of $\bar{y}_{max} = 2.5991$ at time $\tau_{peak} = 735.69$ (2718.4 r.p.m. i.e., $\Omega_{peak} = 1.0611$) indicated by dotted vertical line ($p-p$) in the figure. This shows that the peak response is reached after the speed corresponding to uncracked natural frequency (2562 r.p.m. i.e., $\Omega = 1$) of the rotor due to acceleration of the rotor, which is a well-known fact. In case of accelerating uncracked rotor, the peak response $\bar{y}_{max} = 1.69$ is

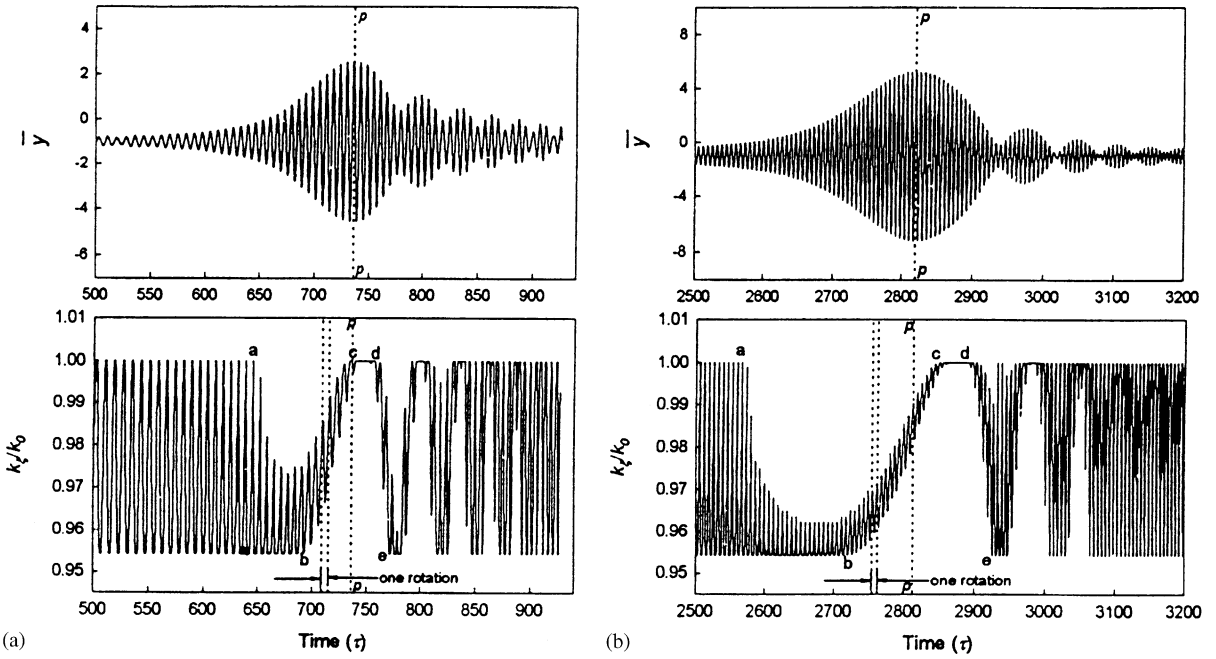

Fig. 3. Dimensionless rotor displacement and stiffness variation showing breathing behaviour during acceleration ($\bar{a} = 0.3; \beta = 0$): (a) $\lambda = 0.0014$; (b) $\lambda = 0.000347$.

Table 1
Peak response and speed at which it is observed for different acceleration rates

	$\lambda = 0.0014$		$\lambda = 0.000347$		$\lambda = 0.0$	
	$\bar{y}_{max}$	Ω	$\bar{y}_{max}$	Ω	$\bar{y}_{max}$	Ω
Uncracked rotor ($\bar{a} = 0.0$)	1.69	1.0694	2.79	1.0314	—	1
Cracked rotor ($\bar{a} = 0.3$)	2.5991	1.0611	5.2272	1.0185	—	0.9768

observed at $\tau_{peak} = 741.6$ (2740 r.p.m. i.e., $\Omega_{peak} = 1.0694$). Thus the speed at which peak response is observed is lowered from $\Omega_{peak} = 1.0694$ to 1.0611 due to the presence of crack in the accelerating rotor (Table 1). The reduction in the critical speed due to crack is 0.8%. This is in accordance with previous findings (e.g., Wen and Wang, 1988), which noted that the change in critical speed due to crack is marginal (less than 5%) and hence cannot be used for crack detection.

The figure also shows rotor stiffness variation as the rotor accelerates through critical speed. The stiffness values evaluated during the elaborate solution procedure of finding the response for breathing crack model are stored during each time step. The stiffness ratio k_ξ/k_0 is plotted in conjunction with the response to study the breathing behaviour of the cracked rotor during passage through the critical speed as the breathing is directly linked to the stiffness variation. The ratio $k_\xi/k_0 = 1$ indicates closed state of crack as k_ξ corresponding to the closed state of crack is

equal to k_0. Similarly $k_\xi/k_0 = 0.9542$ indicates that the crack is fully open since for a fully open crack the k_ξ value drops from k_0 to a minimum. It may be noted that k_ξ takes minimum value when the crack is fully open, since the fully open crack reduces the stiffness of the cracked rotor to minimum. The partially open crack has stiffness less than that of the fully closed crack and more than that of the fully open crack. Thus, any value of k_ξ/k_0 in the range 0.9542 to 1 indicates partially open/close condition of crack. The crack is breathing before it approaches critical speed zone, opening fully and then closing fully in each rotation (Fig. 3a). As it approaches the critical speed zone (say $\tau = 625$–800), the crack tends to open from $\tau = 645$ ($\Omega = 0.9343$) onwards denoted by position 'a' in the figure, the amount of open part of the crack increasing after each rotation. It remains partially open (fluctuating between fully open to partially open state in each rotation) up to $\tau = 687$ ($\Omega = 0.994$) denoted by position 'b' in the figure, after which it exhibits a tendency to close. However it continues to breathe in each rotation neither closing completely nor opening fully. The amount of closed part of the crack continues to increase after each rotation, as the rotor approaches peak response position $\tau_{peak} = 735.7$ ($\Omega_{peak} = 1.0611$) indicated by dotted vertical line ($p-p$). It closes completely at $\tau = 738.9$ marked by 'c' in the figure just after the peak response, stays closed up to $\tau = 757.5$ marked 'd' in the figure. It again opens, rapidly approaching fully open state (position 'e'), stays fully open for a duration of about $\Delta\tau = 6$ and continues to close and open (not in each rotation) till the usual breathing (fully open to fully closed state in each rotation) commences at $\tau = 910$. This rapid opening and closing behaviour (from $\tau = 740$ to 910) after the peak response is reached can be related to beating observed in the rotor response after the rotor crosses the critical speed. This beating in the rotor response after it crosses the resonant speed is due to the interaction of a free vibration at the system natural frequency and the forced vibrations at the instantaneous operating speed [22]. Such beating in the cracked rotor response during coast up operation has also been reported by Wen and Wang [8].

Effect of acceleration rate on the peak response and breathing behaviour is studied. Fig. 3b shows rotor response and breathing behaviour for low acceleration rate of $\lambda = 0.000347$. In this case the peak response is much larger than that obtained with higher acceleration rate ($\bar{y}_{max} = 5.2272$ with $\lambda = 0.000347$ as against $\bar{y}_{max} = 2.5991$ with $\lambda = 0.0014$). The peak response is observed at $\tau_{peak} = 2820$ ($\Omega_{peak} = 1.0182$). The uncracked rotor response with this slow acceleration is found to be maximum $\bar{y}_{max} = 2.79$ at $\tau_{peak} = 2857.4$ ($\Omega_{peak} = 1.0314$). Thus the presence of crack reduces the speed at which the peak response is encountered from $\Omega_{peak} =$ 1.0314 to 1.0182 (a reduction of 1.3%). It may also be noted from the foregoing discussion that the peak response is encountered earlier with lower acceleration rate in both uncracked and cracked rotor cases. This is summarized in Table 1. Comparing the breathing behaviour between low and high acceleration rates, it may be noted that irrespective of the acceleration rate the crack starts to open at almost the same speed ($\Omega = 0.9343$). For higher value of acceleration ($\lambda = 0.0014$), the crack closes just after the rotor attains its peak response (Fig. 3a), whereas for lower value of acceleration ($\lambda = 0.000347$), it closes much later at $\tau = 2860$ ($\Omega = 1.0324$) after the peak response is attained (Fig. 3b). The crack breathing in the critical speed zone (from $\tau = 2500$ to 3000) is little different. With low acceleration rate the stiffness fluctuation is not as large during each rotation as the rotor approaches the speed corresponding to peak response. As the crack starts to close from fully open state from $\tau = 2720$ onwards, the open part of the crack gradually closes after each rotation (Fig. 3b). During each rotation the extent of open/close part of the crack does not vary considerably, the way it does with high acceleration rate. Comparing the variation

of stiffness in a rotation that is shown between the two dotted vertical lines in Figs. 3a and b, it is clear that the fluctuation of stiffness is more intense in case of high acceleration than in lower acceleration case.

Difference between the breathing behaviour presented here and that observed by Plaut et al. [15] should be mentioned here. They used a simply supported rotating Euler–Bernoulli shaft with a switching type transverse crack ($\bar{a} = 0.2$). In their results the crack is shown to remain open right from the start till the peak response position and it is shown to remain closed after crossing the critical speed. However, the results obtained here indicate that the crack opens only when it nears the critical speed zone and it breathes before and after the critical speed zone. Beating phenomenon in the response after the rotor crosses the critical speed influences the breathing pattern after the peak response position.

Instead of changing the stiffness after a gap of 0.001 s, a sample simulation has been carried out with the stiffness modification effected after every 0.0001 s. The integration time step correspondingly reduced by a factor of 10. The result of this simulation indicates that the change of stiffness after 0.0001 s and reduction of integration time step by 10 times has negligible effect on the peak response. Thus the change of stiffness after a gap of 0.001 s and integration time step considered in the earlier simulations (0.00001886 s) is enough to obtain reasonably accurate results. Similarly initial response, when considered to be zero instead of the static deflection, has not shown any noticeable influence on the peak response. Effect of acceleration rate on the peak response is shown in Fig. 4a. Comparison is also made with other crack models and with the response when there is no crack. The figure shows that response for all models is more than the response for the uncracked rotor. Response for switching and open crack model is close to each other for lower acceleration rates, though for higher acceleration rates there is difference in the response values from the two models. Response with breathing model is higher than the response for all other models for all acceleration rates. The difference though is higher for lower acceleration rates. The higher the acceleration rate the lower the response. For lower acceleration rates, the difference between the response of uncracked rotor and cracked rotor is larger, but for higher acceleration rates the difference narrows down.

The effect of deceleration rate on the peak response is also shown in Fig. 4b. Although the general trend is similar to that of the acceleration case, there is a wider difference between

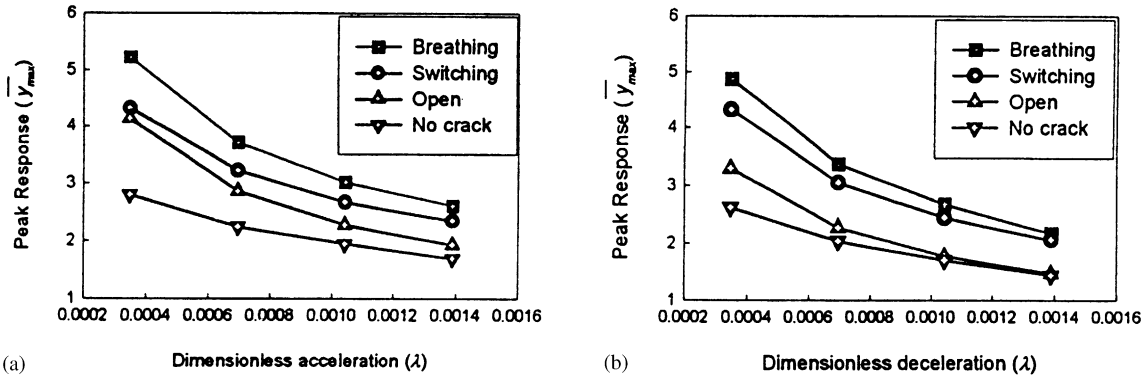

Fig. 4. Effect of acceleration/declaration rate on peak response ($\bar{a} = 0.3, \beta = 0$): (a) acceleration; (b) deceleration.

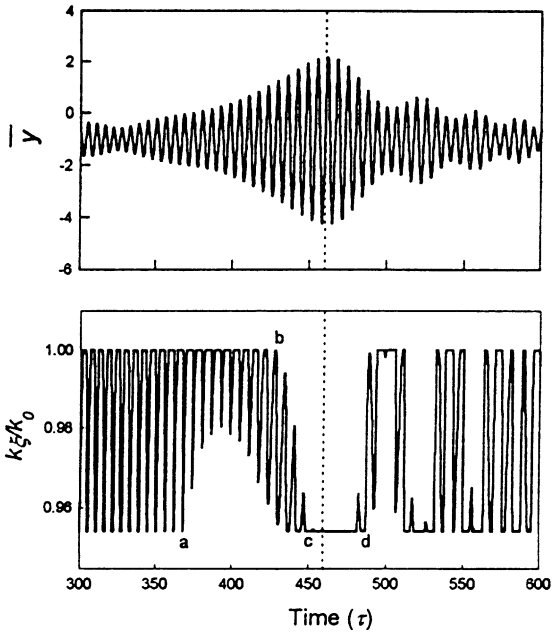

Fig. 5. Rotor response and stiffness variation showing breathing behaviour during deceleration $\bar{a} = 0.3, \beta = 0$, $\lambda = 0.0014$.

response of the open crack model and that of the switching crack model. The breathing crack model still gives a higher response than other models.

Fig. 5 shows the response and the breathing behaviour when the rotor decelerates from $\Omega = 1.56$ to 0.04 with $\lambda = -0.0014$. The peak response of 2.1775 is observed at $\tau_{peak} = 461.2$ ($\Omega_{peak} = 0.9206$) indicated in the figure by a dotted vertical line. The crack in this case tends to close from 'a' to 'b' while approaching the critical speed and then it starts to open. At peak response Ω_{peak}, the crack is completely open. This is in complete contrast to the behaviour of the accelerating rotor where the crack tends to open first and then closes completely near Ω_{peak}. It may also be noted that the peak response in decelerating case ($\bar{y}_{max} = 2.1775$) is lower than that in the accelerating rotor case ($\bar{y}_{max} = 2.5991$).

3.2. Effect of crack depth, unbalance phase and unbalance on peak response

The effect of the crack depth on the peak response obtained using all the crack models is shown in Fig. 6a. The peak response in each case increases with crack depth; the increase is non-linear particularly with the breathing crack model. For all crack depths the breathing crack model gives the largest response. Some notable change in the response appears only after $\bar{a} = 0.1$ and a remarkable change is seen between $\bar{a} = 0.2$ and 0.3. Beyond $\bar{a} = 0.3$ there is a steep rise in the peak response value for the breathing crack model although for other crack models the increase in peak response is not very steep. Figs. 6b–c show comparison of the response variation with crack depth for accelerating and decelerating cases for various crack models. It may also be noted that for

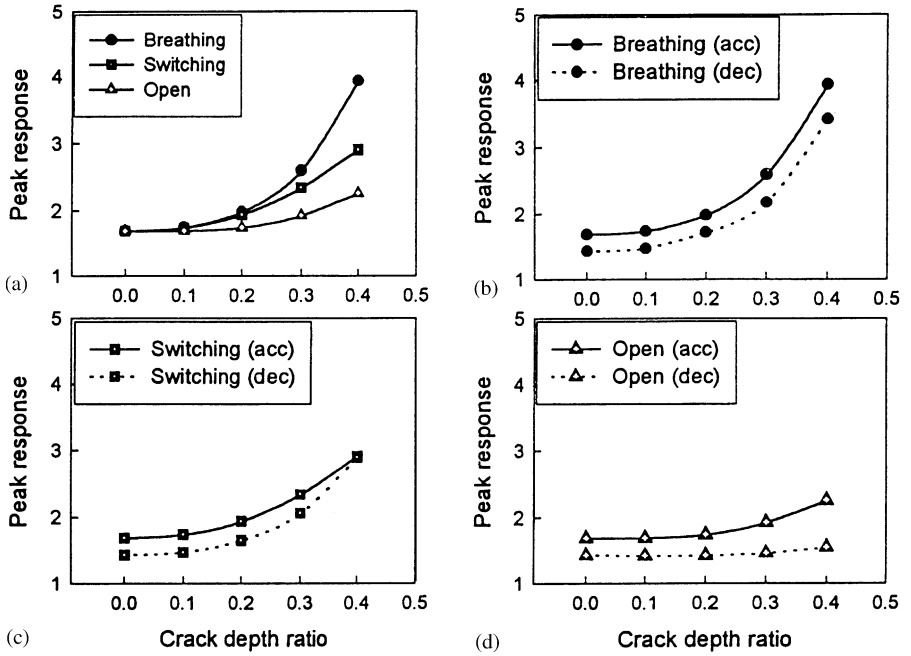

Fig. 6. Effect of crack depth on peak response: $e = 0.1$, $\beta = 0$, $\lambda = 0.0014$. (a) Peak response of accelerating rotor (all models); (b) breathing crack (c) switching crack; (d) open crack.

breathing and open crack models, the peak response during acceleration is larger than that during deceleration for all values of $\bar{a}$ (Figs. 6b and d). For open crack model the peak response during deceleration does not vary substantially with $\bar{a}$. For switching crack, the difference between the peak response during acceleration and deceleration is found constant up to $\bar{a} = 0.3$ (Fig. 6c), beyond which the difference narrows till the accelerating and decelerating rotor response equals at $\bar{a} = 0.4$.

The unbalance orientation angle β, which is the angular position of the unbalance mass relative to the ξ axis in the direction of rotor rotation, has been varied in steps of 22.5° to study its effect on the cracked rotor response. Fig. 7 shows the effect of β on the peak response for $e = 0.1$ (shown in solid curves) and for $e = 0.01$ (shown in dotted curves). For $e = 0.1$ (which is the amount of unbalance considered in most of the simulations reported in this paper), the peak response is maximum for both breathing crack and switching crack near $\beta = 22.5°$ and minimum near $\beta = 157.5°$. Difference in the response of breathing and switching crack models should be noted particularly for $\beta = 0-60°$ and for $\beta = 315-360°$. There is only one maximum and one minimum for the entire range of β values for these two models, whereas there are two maxima (at $\beta = 45°$ and 225°) and two minima (at $\beta = 135°$ and 315°) for the open crack model. The results also show that even the uncracked rotor response is higher than both the switching or breathing crack model rotor response in the range of $\beta = 100-270°$ i.e., when the unbalance is in opposite phase to crack direction. The peak response curve for the uncracked rotor is a straight line.

The above analysis is repeated by reducing the unbalance to $e = 0.01$ from 0.1. Obviously the overall response is reduced but not in the same proportion for all models. Fig. 7a clearly shows

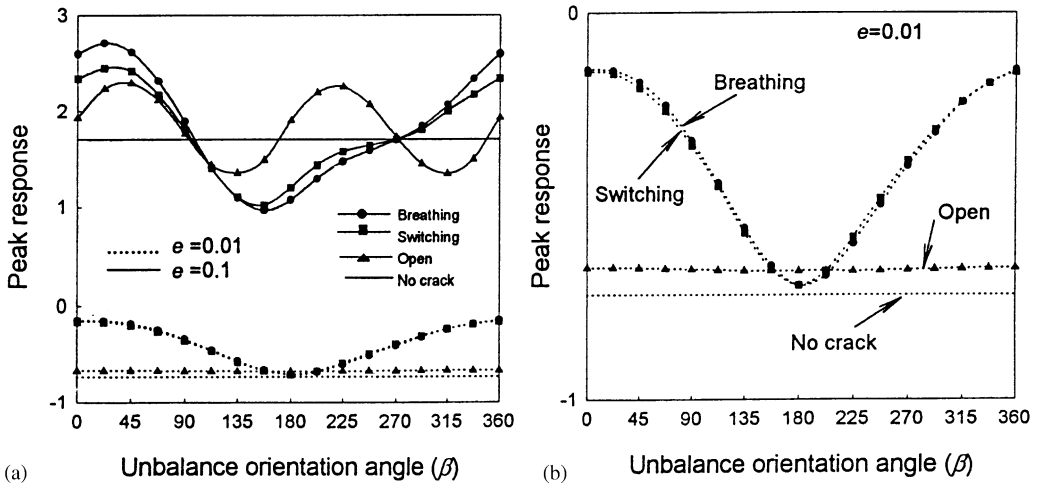

Fig. 7. Variation of peak response with unbalance orientation angle for different crack models and unbalance eccentricity ratio ($\bar{a} = 0.3, \lambda = 0.0014$): (a) $e = 0.1$ and $e = 0.01$; (b) magnified view for $e = 0.01$.

that the open crack model now gives the lowest response compared to the breathing and the switching crack models irrespective of the orientation angle β except near $\beta = 180°$. The peak response curve for the open crack rotor is almost a straight line similar to the uncracked rotor except with larger amplitude. This is clear from Fig. 7b that shows a magnified view of the peak response curves for all models for $e = 0.01$. For breathing and switching crack models, the maximum response position is still at $\beta = 22.5°$ (although not clearly evident from the figure) and the minimum response position is shifted to $\beta = 180°$. In addition, the uncracked rotor response is lower than the response with all the crack models for all the values of β. This shows the effect of amount of unbalance on the peak response variation with β.

From Fig. 7 it is clear that the amount of unbalance influences the response variation with β. This is more evident in Fig. 8 which shows the peak response variation with β in the form of a polar plot for different crack depth ratios and two unbalance values ($e = 0.01$ and 0.9). It is clear that the crack depth ratio and unbalance together influence the relative position of amplitudes of peak response for different crack models. For $\bar{a} = 0.2$ and $e = 0.01$ (Fig. 8a), breathing and switching crack models gave higher response compared to the open crack and uncracked rotor response except for $\beta = 120°$ to $240°$. The peak response is maximum at $0°$ and minimum at $180°$. The uncracked rotor response is almost the same as that of the open crack model, whereas the response for the switching crack model is same as the breathing crack model. For this value of $\bar{a}$, influence of unbalance can be clearly noticed as with higher unbalance of $e = 0.9$ (Fig. 8b) the peak response is maximum at $22.5°$ and minimum at $157.5°$. The range of β for which the uncracked rotor response is higher than the breathing/switching crack model response is now increased ($\beta = 90-225°$). The open crack model response begins to show its typical dumbbell shaped response variation similar to the one shown by Henry and Okah-avae [11]. For a deeper crack ($\bar{a} = 0.4$) and a lower unbalance (Fig. 8c) all the crack models show higher response than the uncracked rotor irrespective of the value of β. In this case the breathing crack model shows larger response than the switching model particularly for $\beta = 0-90°$. For this crack depth, Fig. 8d

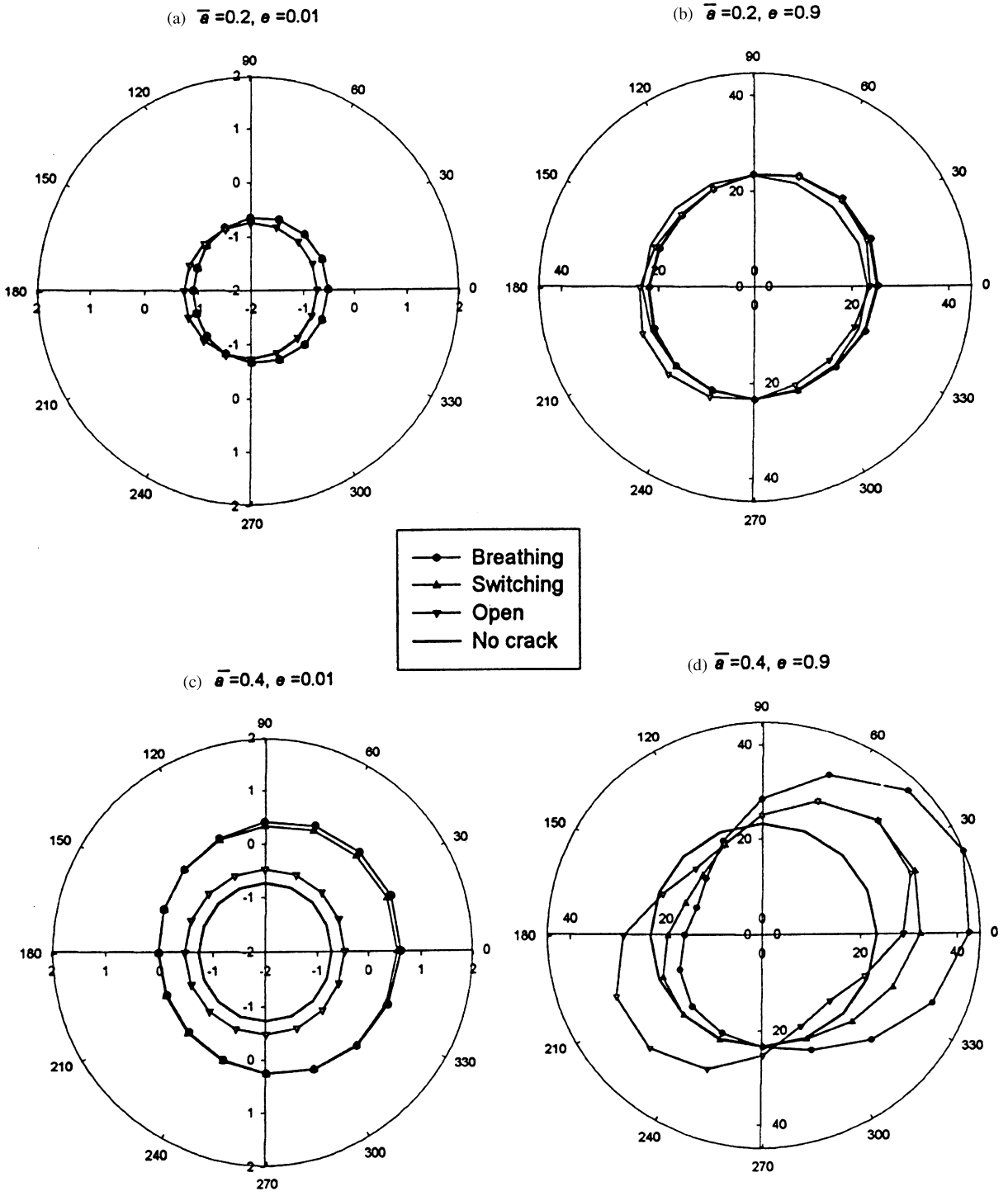

Fig. 8. Variation of peak response with unbalance orientation angle for different combinations of crack depth ratio and unbalance eccentricity ratio.

shows the effect of higher unbalance ($e = 0.9$) where the switching and breathing crack gives higher response than other models when unbalance is in phase with crack direction and lower response when the unbalance is out of phase with crack direction. When the unbalance is in phase with crack, the difference between the breathing and the switching crack models is substantial.

The variation of the peak response with β at the critical speed for the breathing and the switching crack models can be explained. The reduction of peak response occurs for $\beta = 90-270^\circ$, where the unbalance is in opposite direction to that of the crack. The uncracked rotor response is more than the response of breathing or switching crack models when the unbalance is in phase opposition. Considering the results presented in Fig. 8c for very low unbalance value ($e = 0.01$), it may be concluded that the response of cracked rotor is always higher than that of the uncracked rotor. The addition of unbalance influences the response by increasing it when the unbalance is in phase with crack and by reducing it when the unbalance is in opposite phase relative to crack. In this regard one interesting observation by Mayes and Davis [6] may be recalled. Using a very simplified approximation they have shown that the effect of crack is equivalent to adding an out of balance force at an angle β to initial unbalance. Thus when the unbalance is in phase with the crack direction, both unbalance force and this out of balance force representing the crack work in tandem. However when the unbalance is opposite to crack direction, this 'crack force' works opposite to the initial unbalance. This brings down the cracked rotor response below the uncracked rotor response in which this crack force is absent.

3.3. Effect of crack depth, damping and unbalance phase on breathing behaviour

The breathing behaviour of the cracked rotor is influenced by several parameters. The influence of acceleration rate has already been discussed. Fig. 9 shows effects of some of the important parameters on the breathing of the crack. In each figure the peak response position (Ω_{peak}) is shown by a vertical dotted line. Influence of the crack depth is observed on the breathing behaviour (Figs. 9a and b). For these two cases of crack depths the other parameters assumed are $\beta = 0^\circ$, $e = 0.1$ and $\varsigma = 0.01$. For shallow depths, the crack begins to open much later and then closes completely much before Ω_{peak} whereas for deeper cracks it begins to open much earlier and then closes after Ω_{peak}. The fluctuation of stiffness before Ω_{peak} is more intense for lower depth ratio. For deeper cracks, the crack tends to float open before Ω_{peak} without much stiffness fluctuation. For a lower depth of crack, the crack breathes in a partially open state for comparatively shorter period up to the peak response speed, whereas for deeper cracks the crack tends to remain partially open for a considerable time before the peak response is attained. Breathing in a partially open state means the crack does not close completely ($k_\xi/k_0 = 1$ indicates fully closed state) during one rotation, whereas breathing in a partially closed state means the crack does not open completely during a rotation ($k_\xi/k_0 = 0.9542$ indicates fully open state). Sometimes just before reaching the peak response position the crack breathes without closing or opening completely during a rotation (Figs. 3a and b).

Damping plays an important role in the breathing behaviour of crack (Figs. 9c and d). Two cases of damping values are investigated ($\varsigma = 0.01$ and 0.07). For these two cases of damping values, the other parameters used are $\bar{a} = 0.3$, $\beta = 0^\circ$ and $e = 0.1$. For a fairly high value of damping ($\varsigma = 0.07$) the crack breathes (during every rotation) all through the critical speed zone instead of showing a usual partially opened condition before reaching Ω_{peak} and subsequent

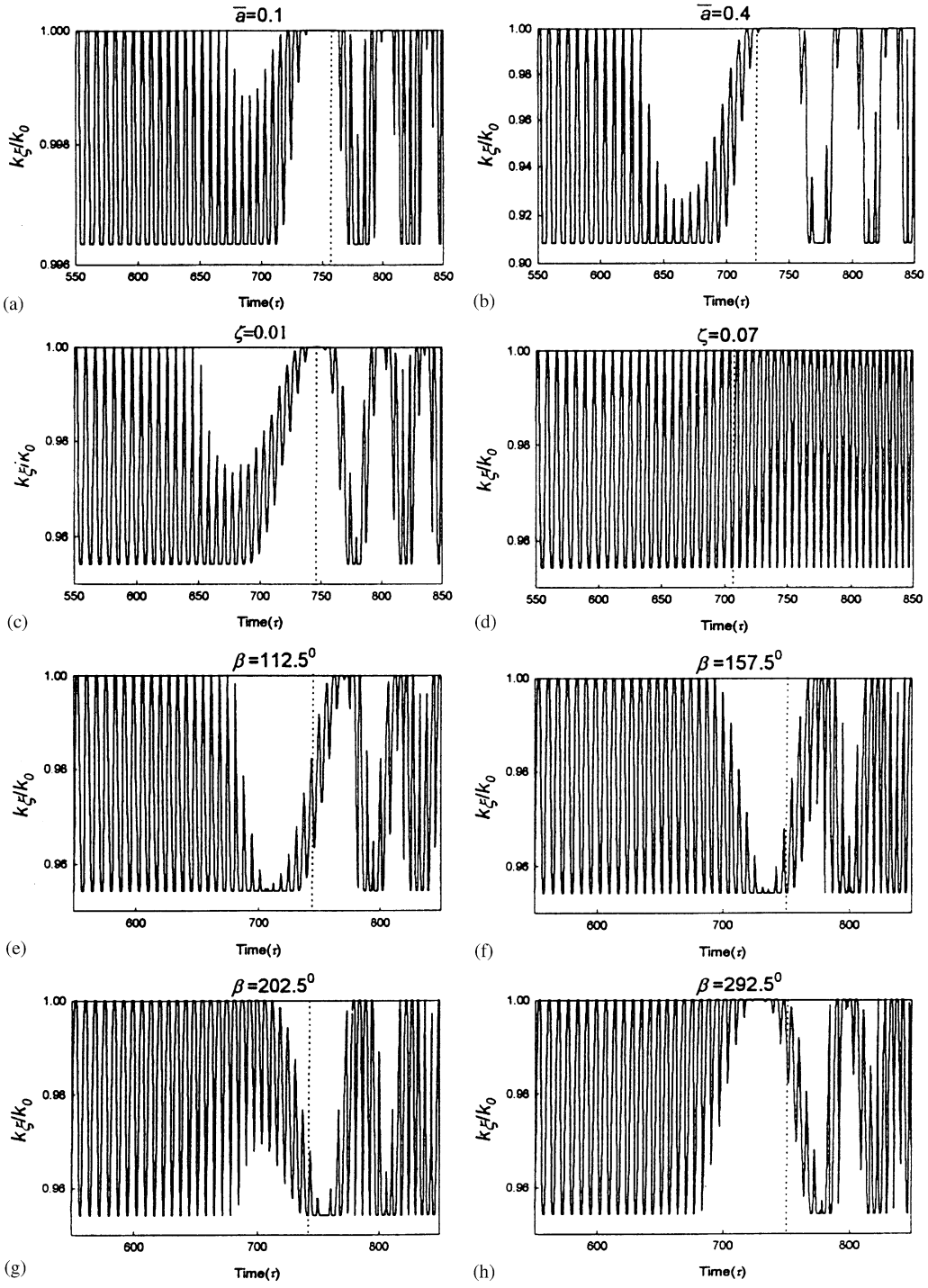

Fig. 9. Effect of various parameters on crack breathing (stiffness variation). Effect of depth of crack (a,b); effect of damping (c,d); effect of unbalance orientation angle (e–h).

open-close pattern related to beating as obtained with lower order of damping ($\varsigma = 0.01$). Similarly for higher damping value the maximum peak response is found to be at $\beta = 45^\circ$ instead of at $\beta = 22.5^\circ$. It may be noted that for shallow depths and higher damping, the breathing observed at speeds away from the critical speed continues even in the critical speed zone and the linear model instead of the response dependent non-linear model could be used in such cases. In case of linear model, the stiffness variation is assumed sinusoidal and dependent only on the rotor angular position rather than on the rotor response. Thus during each rotation, the crack opens fully and closes fully even near the peak response region. This type of crack breathing is not seen in the results with the non-linear models of this study. Both switching and breathing crack models discussed in this paper use stiffness variation that depends on the rotor response and hence are non-linear models. Since for higher damping the stiffness variation is gradual from fully open to fully closed crack state throughout the critical speed region, linear crack model using sinusoidal stiffness variation can be used in such cases.

When the angle β is varied (for $\bar{a} = 0.3$, $e = 0.1$ and $\varsigma = 0.01$), there is a marked change in the breathing behaviour of the cracked rotor (Figs. 9e–h). When $\beta = 22.5^\circ$, the tendency of the crack is to close just after peak response, after remaining partially open before peak response (Fig. 3a). As the angle β is increased (till $\beta = 157.5^\circ$), the crack breathes (from fully open to fully close state in one rotation) up to close to peak response position before starting to open. The time for which the crack remains partially open before the peak response reduces. However when $\beta \geqslant 112.5^\circ$, the crack shows a tendency to remain open near peak response position and it closes much later after peak response. At 157.5° the breathing is considerably intense in the critical speed zone and the open/close pattern related to beating after Ω_{peak} is not seen. After $\beta \geqslant 180^\circ$ the crack shows a tendency to remain closed or partially closed before peak response and it tries to open just after the peak response in contrast to its behaviour at $\beta = 0^\circ$. At $\beta = 292.5^\circ$ the crack is fully closed before the peak response. For $\beta \geqslant 337.5^\circ$, the stiffness variation pattern reverts back to that corresponding to the case when $\beta = 22.5^\circ$.

4. Response during passage through subcritical resonances

Response of the cracked rotor is studied as it coasts up past various subharmonic resonances. When the open crack model is used, the response failed to generate any subharmonic resonance except near $\frac{1}{2}$ the critical speed. At this speed, the second harmonic component was found very strong (several orders of magnitude of first harmonic component). The open crack model at speeds near 1/3rd or 1/5th critical speed does not generate any higher harmonic component except the 2X. However when other models of crack are used results were quite different. Figs. 10i–iii show response of the cracked rotor for breathing crack model while passing through 1/5, 1/3 and 1/2 of the critical speed respectively. These signals clearly indicate predominant fifth, third and second harmonics while passing through the respective subcritical resonances. Frequency domain signal at 1/5th critical speed (Figs. 10c and d) show fifth harmonic component. The 5X frequency component is weak in vertical direction than in the horizontal direction, which is also evident from the time domain signal (Figs. 10a and b). This feature is also seen from the 3X component in vertical and horizontal directions in the frequency domain signal at the 1/3rd critical speed (Figs. 10g and h). Near $\frac{1}{2}$ the critical speed the second harmonic component is very strong, both in

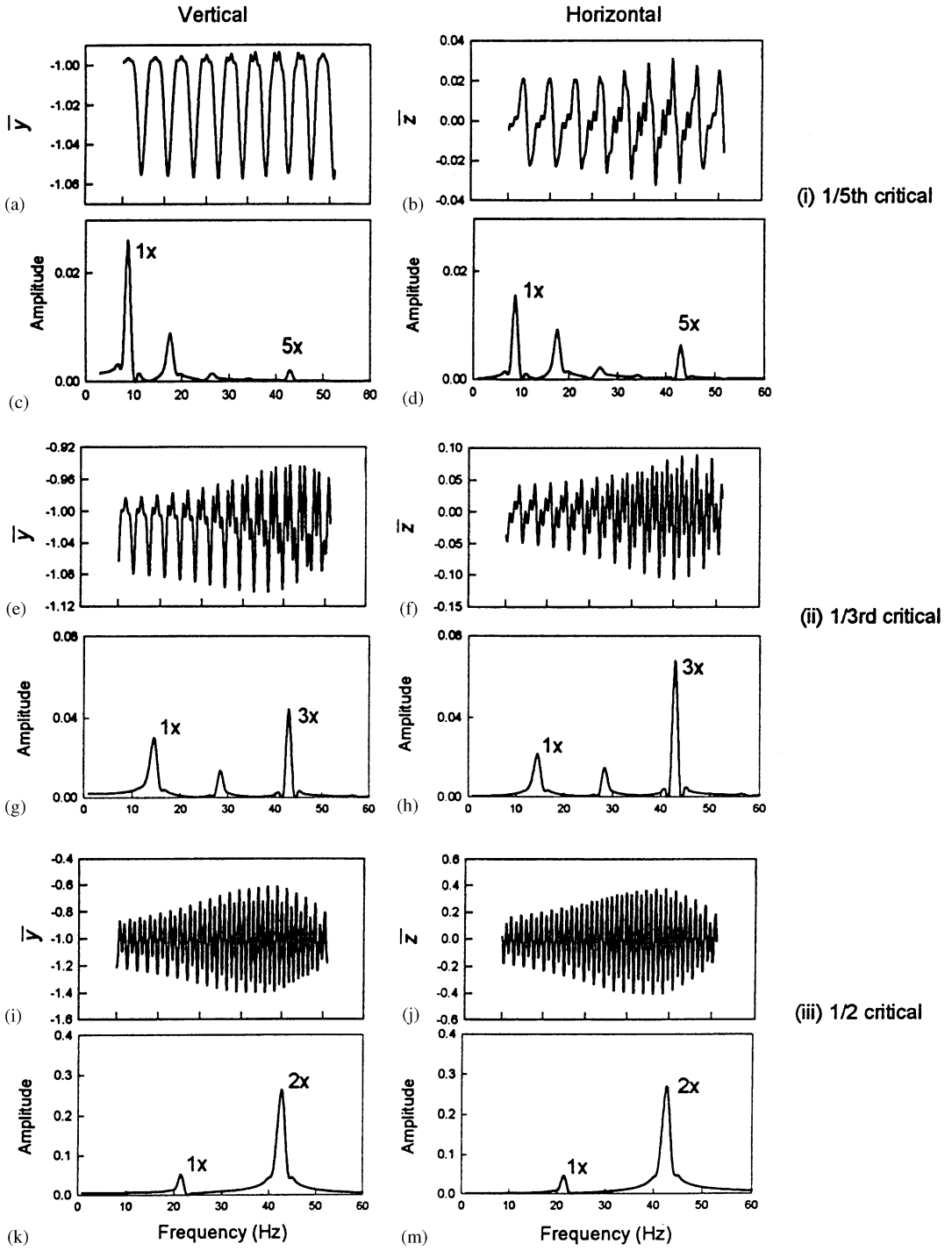

Fig. 10. Response of the cracked rotor while passing through (i) 1/5 (ii) 1/3 and (iii) 1/2 critical speed (breathing crack model).

the time domain (Figs. 11j and k) and frequency domain signals (Figs. 11l and m). However the difference in the vertical and horizontal spectrum is not substantial. Fig. 11 shows the rotor response for switching crack model as it passes through 1/5, 1/3 and 1/2 of the critical speed. At 1/5th critical speed, both the vertical and horizontal signal show equally prominent fifth harmonic component (Figs. 11c and d). At 1/3rd critical speed, the 3X component is found almost eight times stronger in horizontal direction (Figs. 11g and h). At $\frac{1}{2}$ the critical speed the frequency spectra are exactly similar to those obtained with the breathing crack model. This observation is in agreement with the conclusion of Jun et al. [18] that at $\frac{1}{2}$ the critical speed, the breathing and switching crack models yielded similar results. Comparing the results of the breathing and switching crack models, it may be noted that the higher harmonics (5X in the case of 1/5th critical speed and 3X in the case of 1/3rd critical speed) in the case of switching crack model are much stronger than those in the case of breathing crack model. However 2X harmonic component during passage through $\frac{1}{2}$ critical speed is same for both these models.

It may be noted that at subcritical resonances, the stiffness variation influences the frequency composition of the response and this in turn influences the response during the passage through subcritical resonances. For the open crack model the stiffness asymmetry being constant in rotating co-ordinates, the stiffness varies twice in a rotation and the variation being continuous, this model obviously generates a dominant 2X component of vibration under the influence of gravity and no higher harmonics are observed. However in case of the switching crack model, due to sudden switching of the stiffness in the rotating co-ordinate system from fully open to fully closed state, the stiffness change is abrupt giving rise to higher harmonics apart from the second harmonic component of vibration (Fig. 11). In case of the breathing crack model the stiffness in rotating co-ordinate system is not constant (as in open crack model) but there is a continuous variation in stiffness in rotating co-ordinate system; the exact variation depending on the rotor's response. Here also the response contains higher harmonics apart from 2X (Fig. 11).

Orbit plots of cracked rotor as it passes through subcritical resonances are also studied. There has been fewer reported works dealing with the orbital analysis of the cracked rotor passing through the subcritical resonances. The work of Nilsson [3] and Bosmans [23] emphasized the need to observe the phase change as the rotor passes through the resonance. Wen and Wang [8] and Wang et al. [1] have shown analytically that change of phase does occur across the subcritical speeds. Schmied and Kramer [24] discussed the amplitudes and phase angles of the harmonics at fraction critical speed. They discussed orbits only at 1/3 critical speed for in-phase and out-of-phase location of the unbalance relative to crack. Muszynska [25] discussed the differences in the rotor vibrational response components 1X and 2X in misaligned and cracked rotors. She also suggested that orbit shape could change depending on relative amplitude ratio of 1X and 2X as well as phase angle. However authors could not find any analytical study dealing with changes in orbit plots using cracked rotor response during passage through both 1/2 and 1/3rd critical speeds and any experimental study regarding change in orbit plots across subcritical resonances. In the present work, an attempt is made to study the orbits and changes in the orientation of orbits as the cracked rotor crosses the subcritical resonance. The focus is on utilising the phase change across the subcritical resonances that shows up in the change of orbit orientation.

A cracked rotor with depth of $\bar{a} = 0.3$ is coasted up through all the subharmonic resonances and the response near the peak at these resonances is analyzed. Fig. 12a shows the time domain response of the cracked rotor during the passage through 1/2 of critical speed. Figs. 12b and c

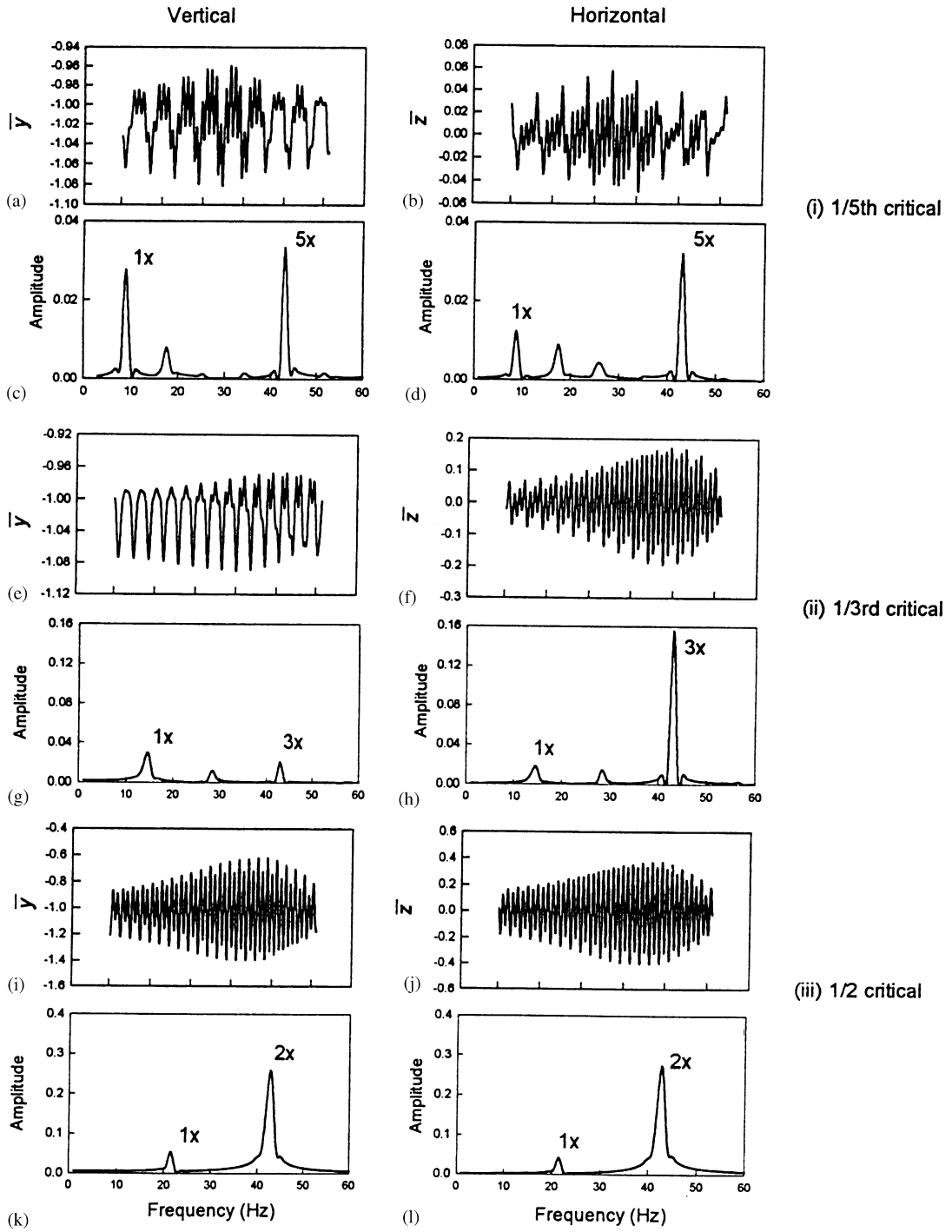

Fig. 11. Response of the cracked rotor while passing through (i) 1/5 (ii) 1/3 and (iii) 1/2 critical speed (switching crack model).

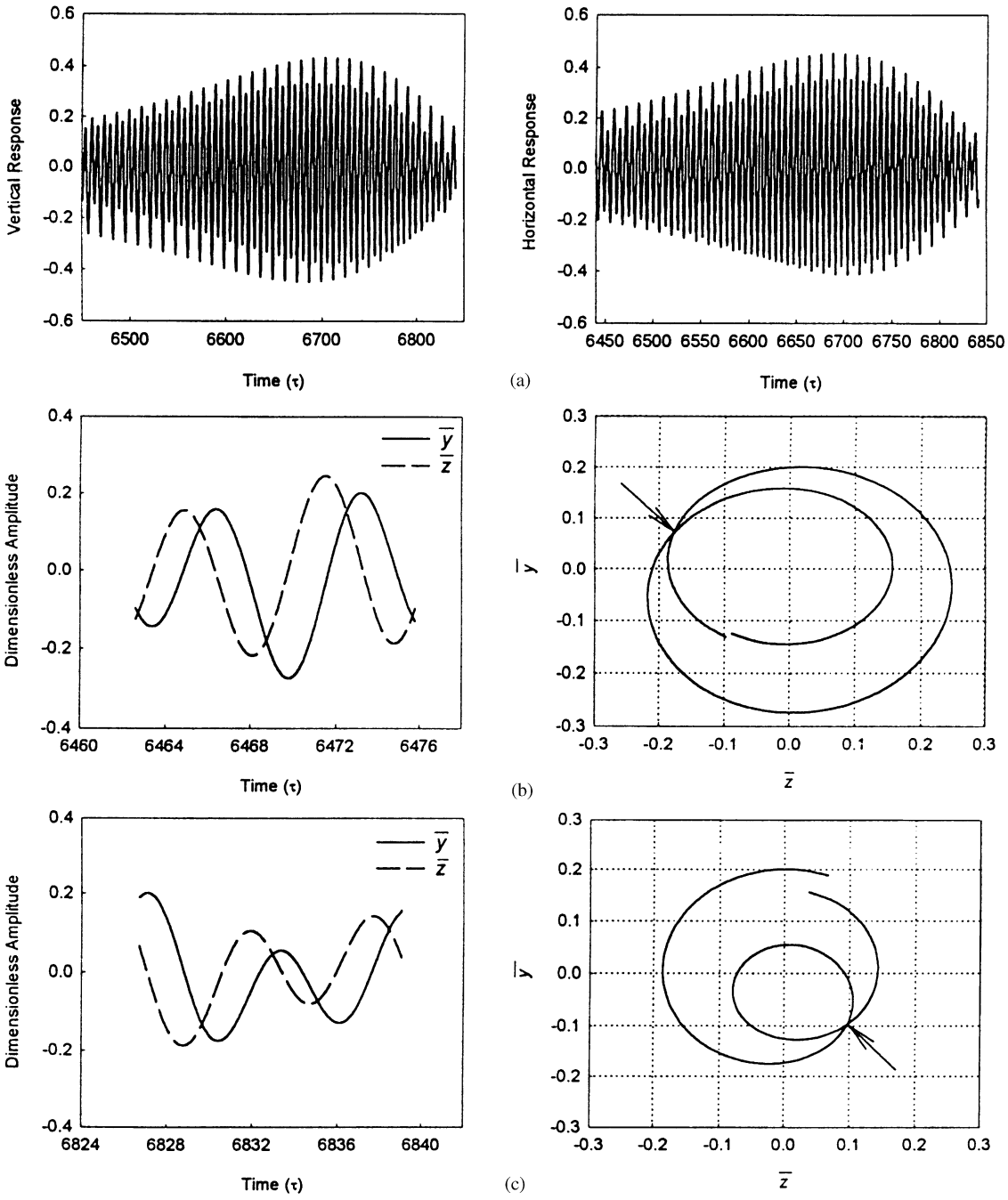

Fig. 12. Time domain and orbit plots during the passage through 1/2 critical speed (analytical): (a) time domain response during the passage; (b) time domain and orbit plot before the 1/2 critical; (c) time domain and orbit plot after crossing 1/2 critical.

respectively show the time domain response and orbit plot before and after the 1/2 critical speed. The change in the orbit orientation is clearly seen. The inner loop that is formed due to dominant second harmonic component, changes its orientation by almost 180° (shown by an arrow in the figure). This change of phase is also evident from the time domain response in horizontal and vertical directions shown in each case. Fig. 13 shows the response of cracked rotor while passing through 1/3 critical speed. Here also the inner loop's orientation clearly changes by about 180°, as the subcritical resonance is crossed.

During passage through 1/5th of the critical speed (Fig. 14), the shape of the orbit changes slightly and the orientation change is not very obvious compared to the earlier cases. However, it may be noted that the orbit that is inclined in the first quadrant before the peak, changes its orientation to a vertical position after crossing the peak response. . The resonance is not very pronounced here, particularly in the vertical direction, as compared to the one observed at 1/2 and 1/3 critical speeds. It may also be observed that the time domain response in vertical direction shows a substantial dip (shown with an arrow) in the middle of one cycle of rotation. This dip is typical of a slowly rotating cracked rotor's response and corresponds to the reduction in the stiffness as the crack opens up completely at around $\theta = 180°$.

The effect of damping on the orbit orientation changes is investigated by increasing the damping from $\xi = 0.01$ to 0.05. With increased damping, the subharmonic resonance corresponding to 1/5th of the critical speed disappeared. The orbit orientation changes are still clearly observed during passage across both 1/3rd and $\frac{1}{2}$ of the critical speed. With the increased level of damping i.e., $\xi = 0.05$, the orbit changes its orientation by about 90°, whereas this change is about 180° for a relatively lower damping of $\xi = 0.01$.

5. Experimental investigations

For verifying the theoretical findings in this study, experiments are carried out on both slotted and cracked shafts. For this purpose a test rig is developed that comprises a cracked/slotted rotor with a central disk, a driving unit, and measurement, signal processing and data acquisition unit as shown in Fig. 15. For experimentation on the rotor simulating an open crack, a slot of width 1 mm is machined on the rotor near the disc using a slitter to a desired depth. For a rotor with real crack, a fatigue crack is induced on the shaft transversely using a three-point-fatigue bending machine. For this purpose a 25 mm diameter shaft is used with a very fine initial slit of width 0.5 mm and depth 1 mm using a jeweler's saw. This is to initiate a fatigue crack at a desired location. The shaft is then placed in the three-point-fatigue bending machine and subjected to cyclic loading. Once the crack propagates to a desired depth, the specimen is machined to a diameter of 15 mm and supported with a bearing span of 640 mm. A disc of mass 1 kg is mounted at mid-span and the rotor is then supported on self-aligning ball bearings.

Due care is taken to minimize the effect of disc ovality and eccentric mounting of the disc. The disc was machined with extreme care using follower and steady rests, after assembling it on the shaft. The disc was assembled on the shaft by shrink fitting. The measurements at the shaft have indicated cross-talk between the vertical and horizontal probes due to smaller shaft diameter. Therefore, measurement on the disc was considered necessary. A sample simultaneous

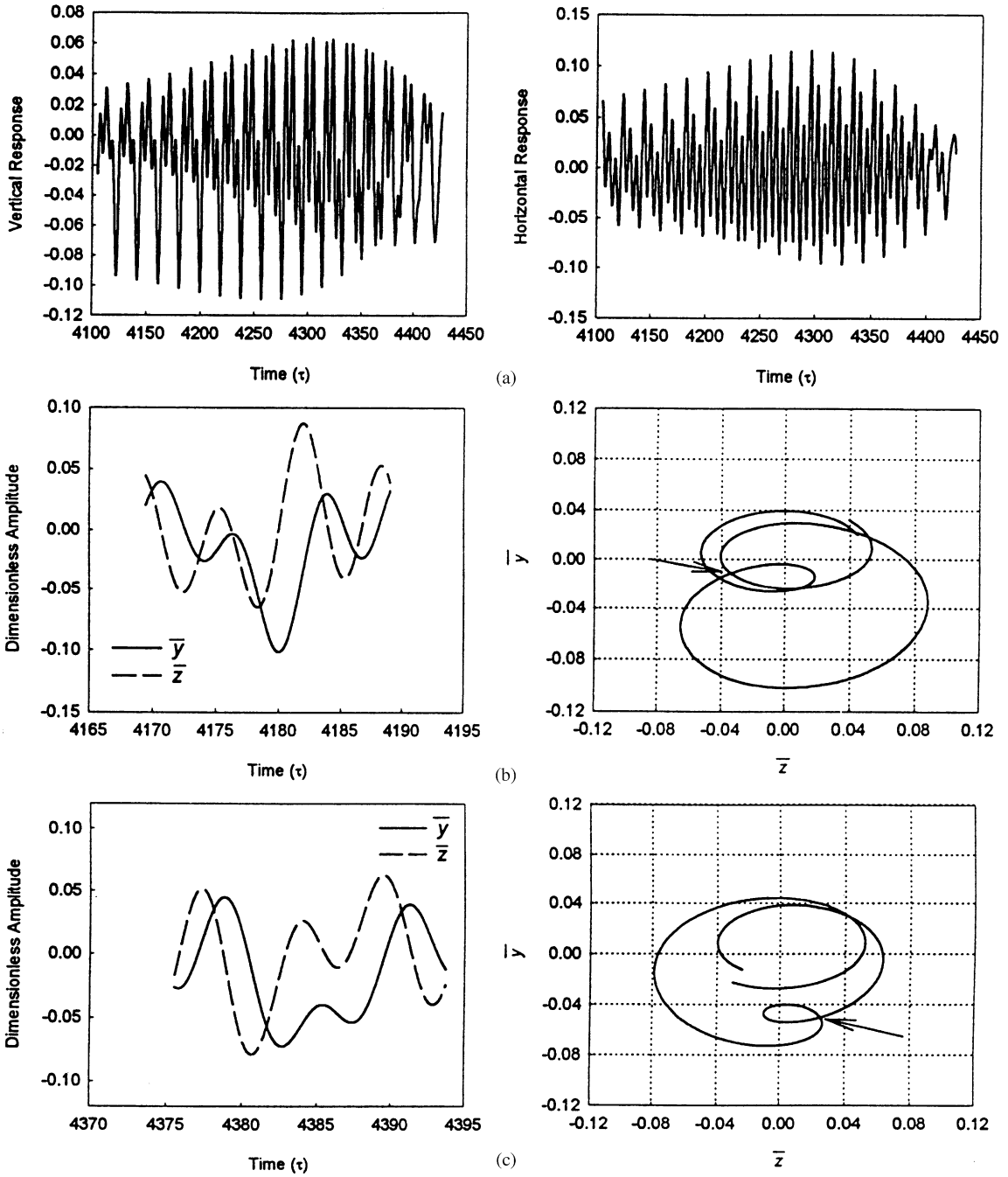

Fig. 13. Time domain and orbit plots during the passage through 1/3 critical speed (analytical): (a) time domain response during the passage; (b) time domain and orbit plot before the 1/3 critical; (c) time domain and orbit plot after crossing 1/3 critical.

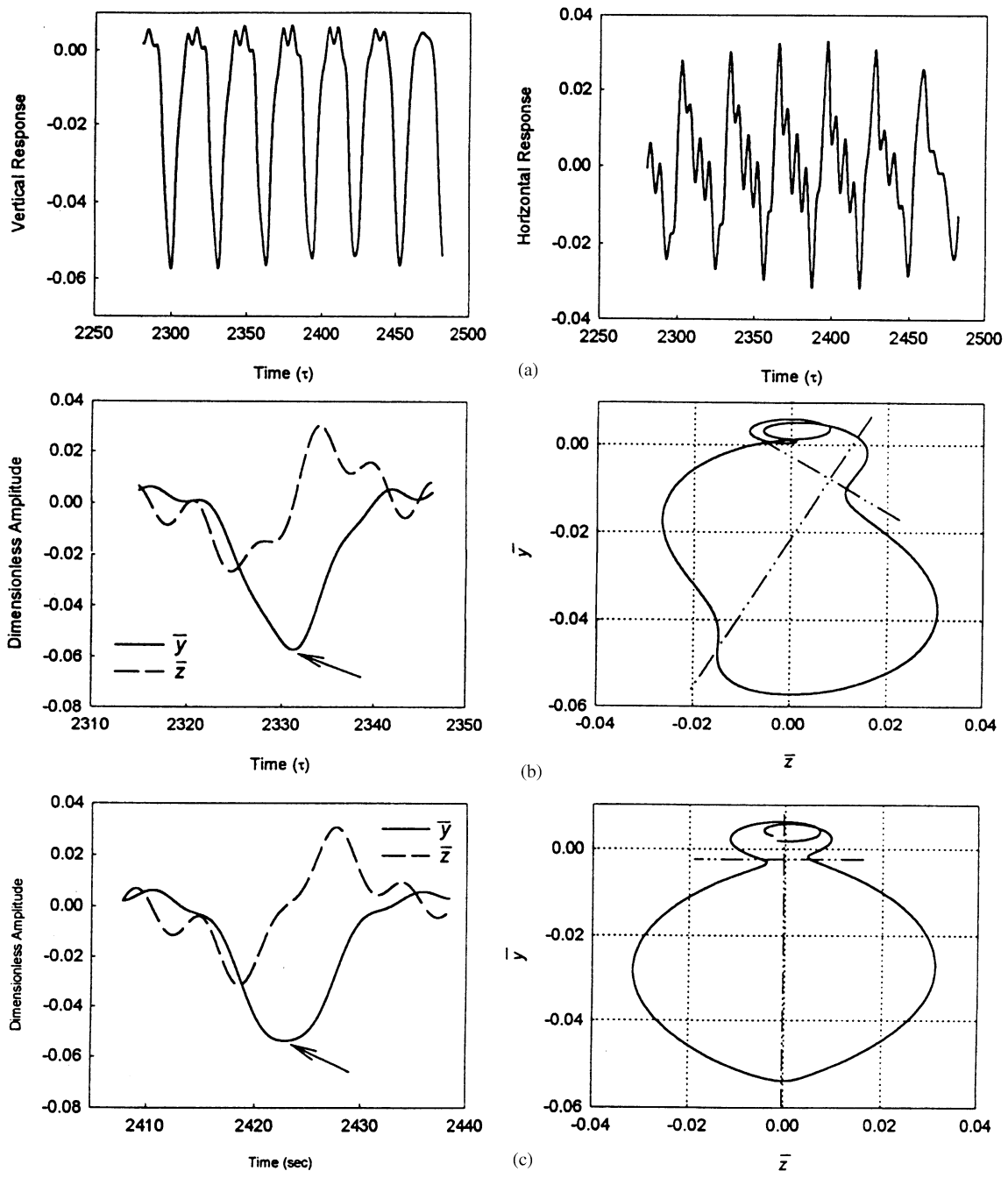

Fig. 14. Time domain and orbit plots during the passage through 1/5 critical speed (analytical): (a) time domain response during the passage; (b) time domain and orbit plot before the 1/5 critical; (c) time domain and orbit plot after crossing 1/5 critical.

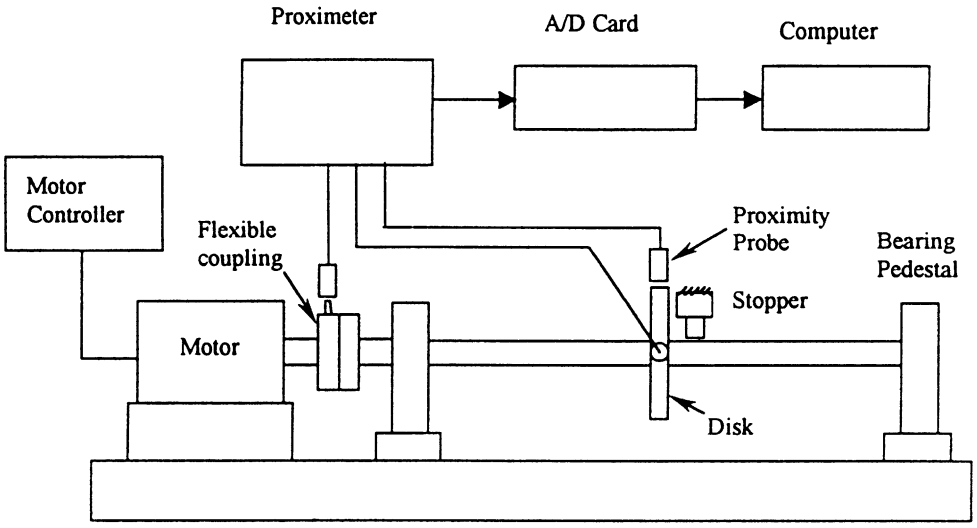

Fig. 15. Test rig with instrumentation.

measurement of vibrations at the shaft and the disc locations has shown good agreement. Therefore, rest of the measurements are made on the disc.

A flexible Lovejoy type coupling connects the rotor with the drive motor which is Seimens make 750 W three-phase induction motor controlled by a Micromaster vector wherein the ramp rate during coast up as well as during run down can be very precisely controlled. The response of the rotor is measured using non-contact type eddy current probes. The signals are conditioned by a proximeter before sending them to the A/D card plugged on to a digital computer. A small Labview™ virtual instrument is developed which facilitates in acquiring and storing the digitized data on the computer. The signals are acquired simultaneously from three proximity probes, two probes at disc location (one each for horizontal and vertical shaft vibrations) and one near the coupling for KeyPhasor signal.

The main objective of the experiments is to validate the peak response variation with unbalance orientation angle for both cracked and slotted rotors and to study orbit orientation changes across subcritical resonances. The effect of amount of unbalance on the response variation is also investigated.

To begin with, a coast-up and rundown operation is performed on a slotted rotor with depth of slot of 3.5 mm ($\bar{a} = 0.23$). This operation is repeated for 16 different unbalance orientation angles (β) in steps of 22.5°. An unbalance mass of 1.6 g is placed at a radius of 50 mm on the disc, giving a dimensionless eccentricity of $e = 0.53$. The coast-up and run-down time domain response is obtained for each β from which the peak response during acceleration and deceleration is obtained. The variation of peak response for this slotted rotor during acceleration and deceleration is shown in Fig. 16a. The variation is not quite as per analytical findings. The two maxima and two minima are not very clear. However one maxima is seen at 225° and two minima are at approximately 100° and 315° respectively. Also, over a small range around $\beta = 0$, the decelerating rotor response is more than the accelerating rotor response. The unbalance is increased from $e = 0.53$ to 0.79 and the experiments are repeated. The variation of peak response

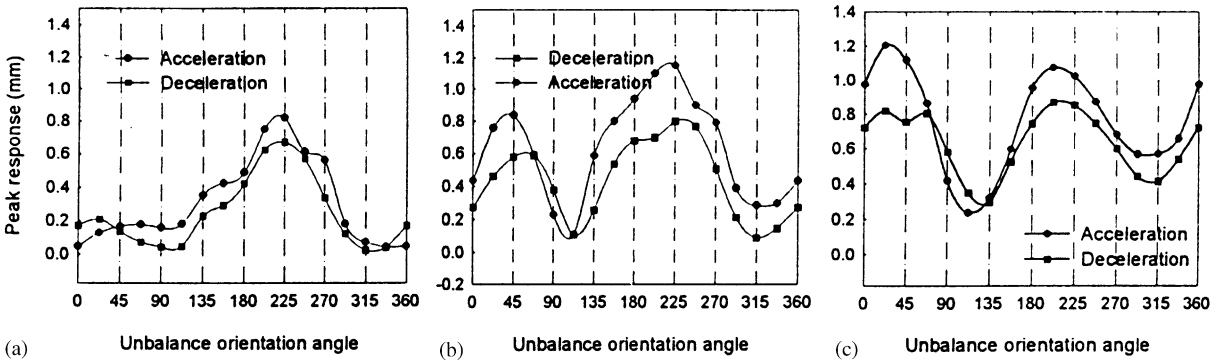

Fig. 16. Variation of peak response with unbalance orientation angle for open crack (slotted) rotor (experimental): (a) $\bar{a} = 0.23$, $e = 0.53$; (b) $\bar{a} = 0.23$, $e = 0.79$; (c) $\bar{a} = 0.3$, $e = 0.53$.

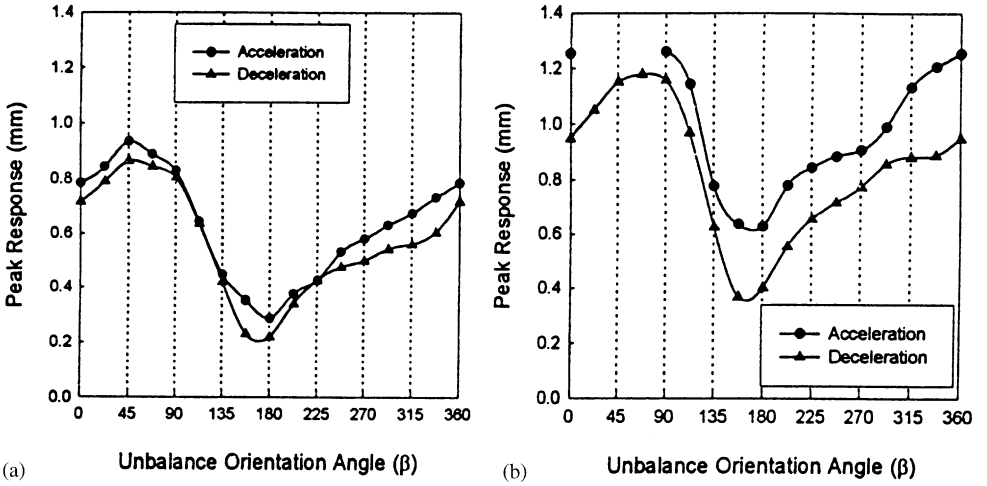

Fig. 17. Peak response variation with unbalance orientation angle for fatigue cracked rotor (experimental) ($\bar{a} = 0.23$): (a) $e = 0.53$; (b) $e = 0.79$.

is now very similar to the theoretical one, having two maxima at about 45° and 225° and two minima at about 135° and 315° (Fig. 16b) respectively. Here the range over which the decelerating response is larger than the accelerating rotor is centred around 90°. This feature is maintained when the slot depth is increased to 4.5 mm ($\bar{a} = 0.3$) approximately. Variation of peak response with phase of unbalance now matches exactly with the theoretical one (Fig. 16c).

For the cracked shaft of approximate depth $\bar{a} = 0.23$, a similar exercise is repeated. Fig. 17 shows the response variation which is quite similar to the theoretically obtained one (Fig. 7). There is one maxima and one minima at $\beta = 45°$ and 157.5° respectively. Similar variation was also observed during deceleration. For a range of β from 90° to 135°, the peak response during deceleration is found to be almost the same as during acceleration. When the same shaft is

operated with a larger unbalance by increasing the unbalance mass ($e = 0.79$ instead of 0.53), the peak response during deceleration is always smaller than that during acceleration (Fig. 17b). For $e = 0.79$, the accelerating rotor response for a range of unbalance orientation angle around 45° could not be obtained because the rotor started vibrating violently and hit the stoppers which were installed for limiting the vibrations of the shaft. However the general trend looks similar to the case with a lower unbalance. In addition the difference between the peak response values during acceleration and during deceleration is more in the present case of higher unbalance compared to the case when the unbalance was lower (Fig. 17a).

Fig. 18 compares the peak response variation (experimental) between the slotted rotor and the fatigue cracked rotor. Fig. 18a shows the comparison for the accelerating rotor case and Fig. 18b shows the comparison for the decelerating rotor case. In both cases a clear distinction can be made between the slotted rotor and cracked rotor from the type of variation of the peak response. The number of maxima and minima for peak response is two each in case of slotted rotor as against one only for the case of cracked rotor. This important feature can be used for distinguishing the response of an asymmetric rotor from that of the cracked rotor. Finally for the slotted rotor the response variation obtained analytically and experimentally is compared in Fig. 19a. The overall response variation is matching qualitatively for both acceleration and deceleration cases. However there is some difference in the amplitudes. The difference between the theoretical and experimental values can be attributed to the damping value used in the analytical simulation. The damping factor used ($\zeta = 0.019$) is based on the time displacement plot during rap test on the rotor. However during the passage through critical speed the large amplitudes in the range of 1 mm have been noted. For such large amplitudes, the same damping value would not be applicable. The stiffening effect at larger amplitudes tends to limit the rotor resonant amplitudes. The peak response at resonance being highly sensitive to the damping value, the actual experimentally observed response has been found to be lower. In addition to the amplitude level, the damping also affects the maximum peak response position as shown in the analytical results of

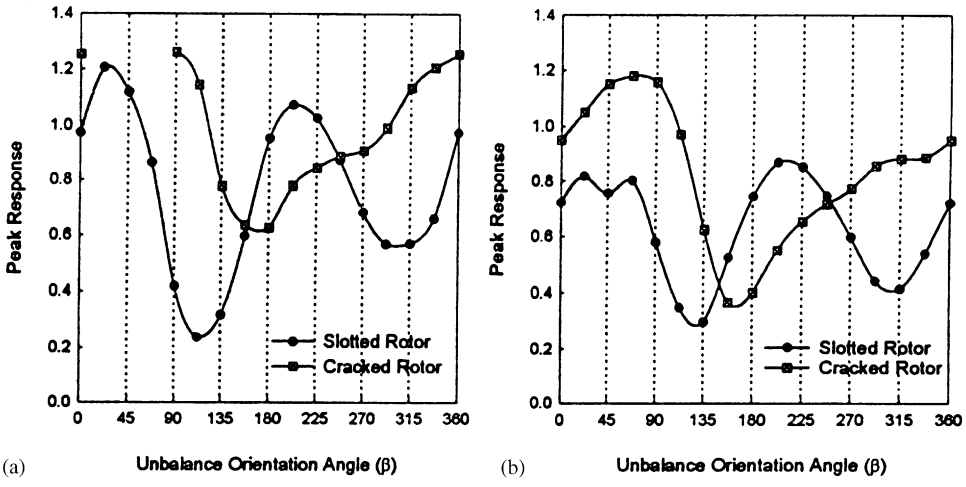

Fig. 18. Comparision of peak response variation (experimental) with β for slotted and cracked rotor ($\bar{a} = 0.23$): (a) accelerating rotor; (b) decelerating rotor.

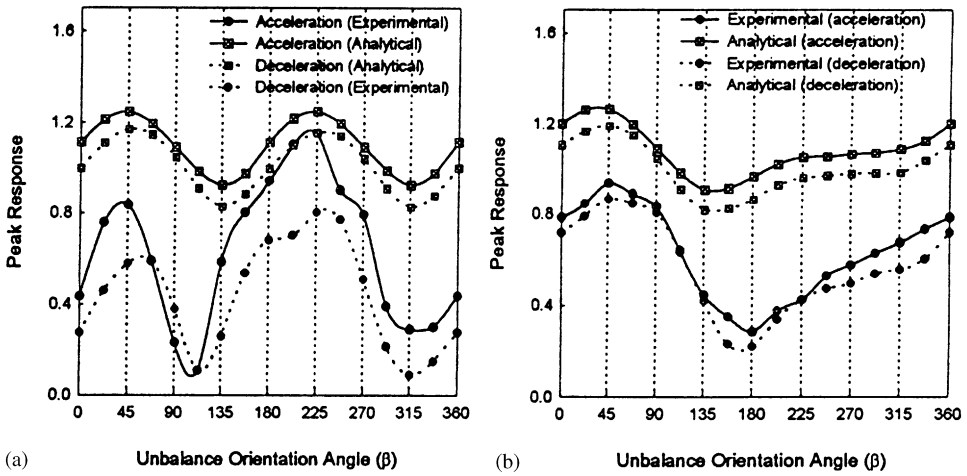

Fig. 19. Comparision of peak response variation between experimental and analytical results for (a) slotted rotor and (b) fatigue cracked rotor.

Section 3.3. The higher level of damping changes the maximum peak response position from 22.5° to 45°. The present experimental observations confirm this fact. Similar comparison between analytical and experimental values is made for the cracked rotor (Fig. 19b). The response variation is qualitatively matching here as well. Problem of high resonant amplitudes with rotor hitting the limit stops was encountered on a rotor with a higher depth of crack ($\bar{a} = 0.37$) and hence experiments for peak response variation could not be carried out.

The present experimental observations on a cracked rotor have established minimum peak response between 157.5° and 180° and maximum peak response at 45°. In most of the earlier investigations [6,14] the value of β was varied in steps of 90° and results extrapolated for other values of β. Variations reported in the literature [5–7,14] (either analytically or experimentally) regarding β corresponding to maximum peak response range from 0° to 90° and for minimum peak response range from 120° to 180° and in some studies [13] maximum is reported at 0 and 180° and the minimum at 90°.

The experiments to verify changes in the orbit plot orientation are also carried out on the cracked rotor as it is coasted up past the subcritical resonances. Two cracked rotors are used in the study, one with crack depth ratio of $\bar{a} = 0.23$ and another one with $\bar{a} = 0.37$. The acceleration rate used is $5.6\,\mathrm{rad/s^2}$. Fig. 20i shows the time domain response and orbit plots of the cracked rotor as it runs-up through 1/2 the critical speed. The looped orbit with one inner loop oriented in the 1st quadrant before 1/2 the critical speed changes its orientation to the 4th quadrant after crossing it. The orientation of the inner loop thus changes by 90°. Although the orbit does not change the orientation by almost 180° as seen in the theoretical studies, the change in the orbit orientation is very clear. Fig. 20ii shows similar plots of the cracked rotor as it coasts up past the 1/3 critical speed. The orbit with two inner loops on the sides is seen oriented almost close to vertical before reaching 1/3 critical speed peak. Just after crossing the resonance, the orbit is more or less oriented horizontally with the inner loops positioned one above the other.

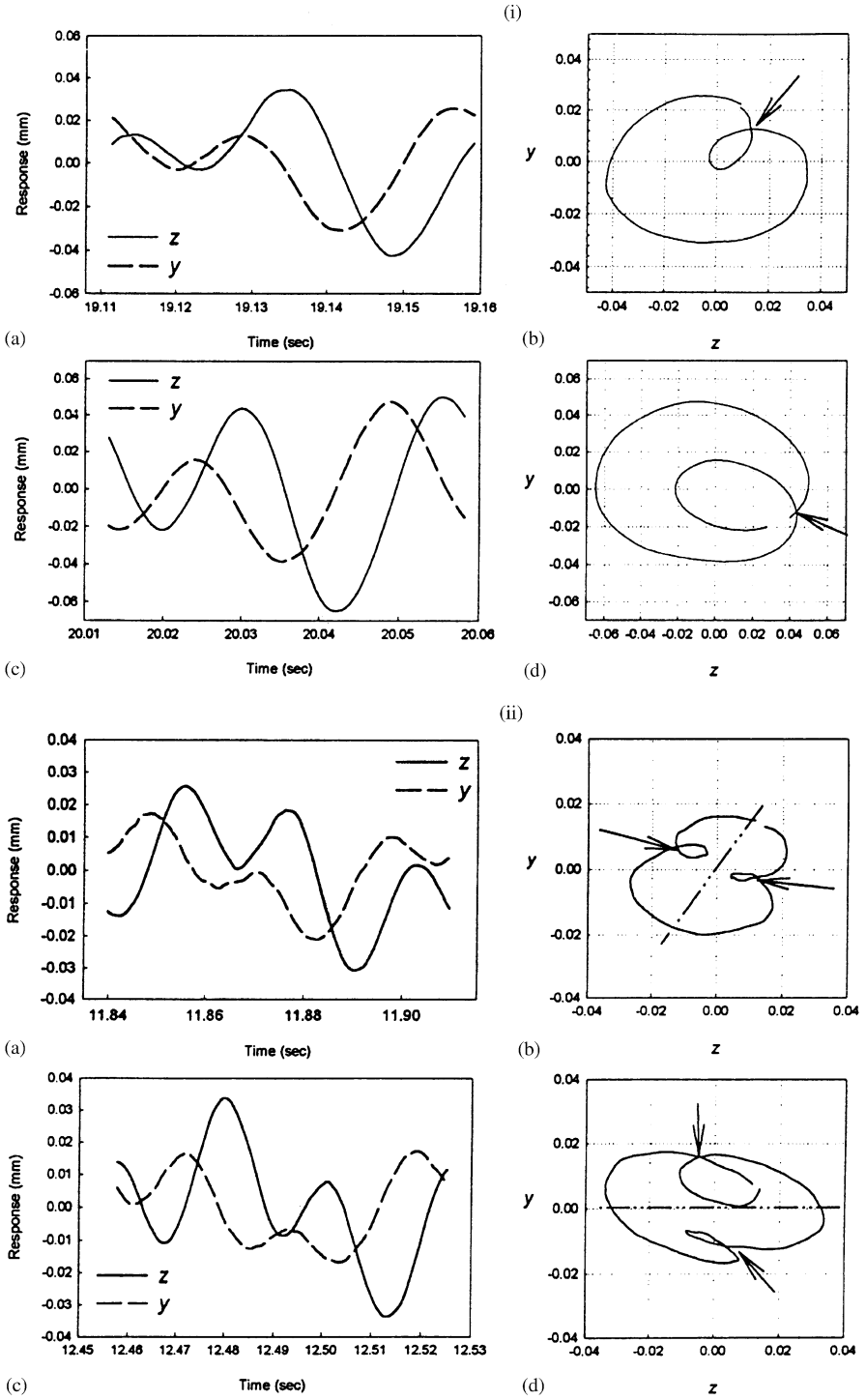

Fig. 20. Time domain and orbit plots during the passage through subharmonic resonances: (i) 1/2 critical speed and (ii) 1/3 critical speed (experimental). $a/D = 0.23$. $\alpha = 5.6\,\mathrm{rad/s^2}$. (a) Time domain response and (b) orbit plot before resonance; (c) time domain response and (d) orbit plot after crossing resonance.

Similar results were obtained with the other cracked shaft with greater crack depth ratio ($\bar{a} = 0.37$). Fig. 21i shows the response of the rotor as it passes through 1/2 the critical speed. Here the orbit orientation is seen to change by about 90° from the second quadrant to first quadrant. Fig. 21ii shows the response of this cracked rotor while passing through 1/3 critical speed. In this case the two loops are much more pronounced and the orientation of orbit changes from the 1st quadrant to the fourth quadrant. The relatively lesser orbit orientation change observed in experimental results compared to analytical results (Figs. 12–14) could be attributed to the higher damping in the system. In the theoretical analysis, it is shown that the damping does affect the change of orientation of orbit plot.

From the time domain response near the 1/2 and 1/3 the critical speed (not shown here), it has been observed that the time for passage through both these resonances is more (almost double) compared to the rotor with lower depth ratio. Thus, for deeper crack the resonance region at 1/2 and 1/3 the critical speed is wider and the rotor tends to stay suspended in the region. In their theoretical investigations on transient vibrations of a cracked rotor near main critical speed, Sekhar and Prabhu [13] noted that for deeper cracks there is no definite critical speed but a zone with severe vibrations. They have also noted that it is difficult for a practical rotor with deeper crack to pass through its critical speed smoothly. The observation that this is also true for subcritical resonances in addition to the main critical speed is another important experimental outcome in the present study.

From practical considerations, it is important to understand the difference in the orbits due to crack and due to misalignment, since the latter is the second most significant cause of generation of 2X component of vibration other than stiffness asymmetry. The orbit plots in misaligned rotors are predominantly with the loops outward (external loops). The response in one direction in this case is dominant with a 1X component and in the other direction has higher harmonics because of the system non-linearity induced by large deflections due to a radial pre-load [25]. In fact the looped orbits in case of misalignment are observed only for severe misalignment and in such cases they are eight shaped with outward loops. With lower to moderate misalignment, the orbits are usually 'banana' shaped (oriented in the direction of misalignment). However the orbit plots in case of cracked rotor (even for quite low crack depth) invariably show internal loops. This is because due to the induced stiffness asymmetry the vertical and horizontal responses are similar in frequency content in the case of a cracked rotor. In misaligned rotors they are substantially different in these two directions due to the directional nature of the preload. Hence a cracked rotor produces circular orbits with internal loops whereas misaligned rotors produce elongated orbits with outward loops. The internal loop in case of actual cracked rotor has also been reported by Jenkins [26]. This difference in orbit pattern could be used to distinguish rotor crack from misalignment apart from the fact that misalignment generates substantial axial vibration response, whereas the cracked rotor response is mostly radial in nature.

The time domain and frequency domain signals of the cracked rotor passing through subharmonic resonances are shown in Fig. 22. The 5X and 3X components are clearly seen in the frequency domain plot in both vertical (Figs. 22c and g) and horizontal directions (Figs. 22d and h). However, the amplitudes of these harmonics are stronger in the horizontal direction compared to the vertical direction confirming the inferences from the analytical spectra (Figs. 10 and 11). Particularly at 1/5th and 1/3rd critical speed, these experimental spectra (Figs. 22c, d, g and h) are

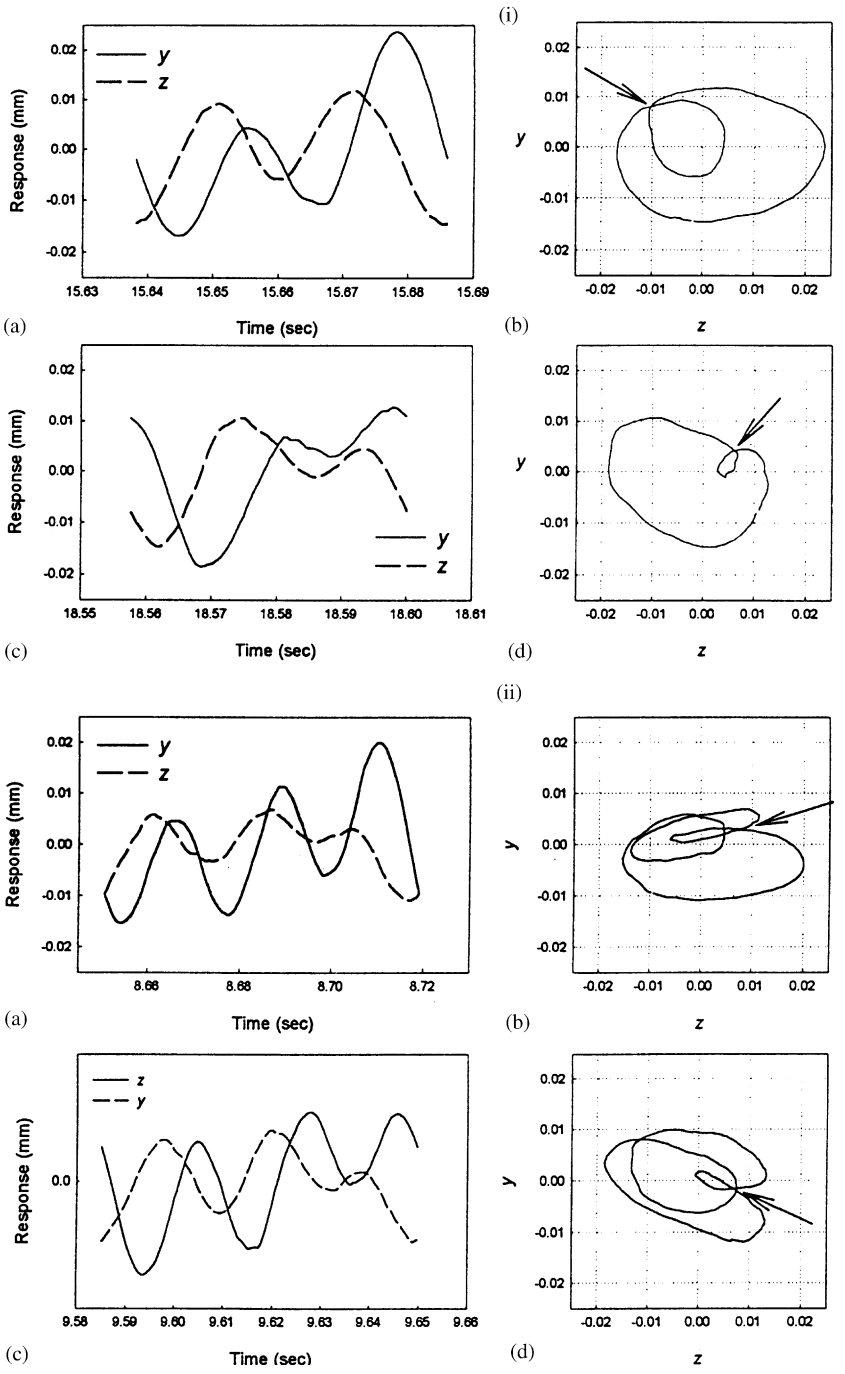

Fig. 21. Time domain and orbit plots during the passage through subharmonic resonances: (i) 1/2 critical speed and (ii) 1/3 critical speed (experimental) ($a/D = 0.37$. $\alpha = 5.6\,\mathrm{rad/s^2}$). (a) Time domain response and (b) orbit plot before resonance; (c) time domain response and (d) orbit plot after crossing resonance.

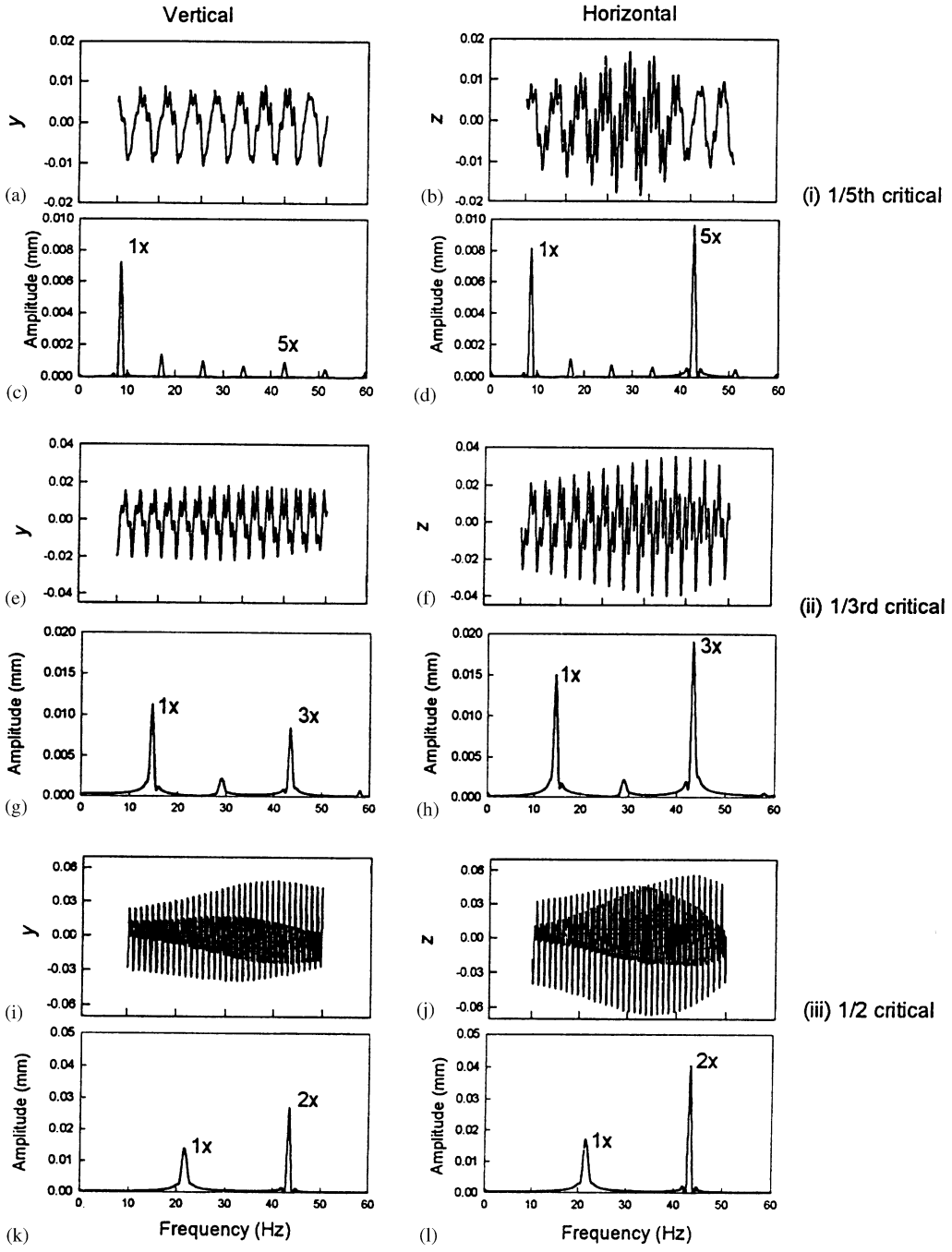

Fig. 22. Response of the cracked rotor while passing through (i) 1/5 (ii) 1/3 and (iii) 1/2 critical speed (experimental).

found closer to the breathing crack model (Figs. 10c, d, g and h) than the switching crack model (Figs. 11c, d, g and h) that predicted the amplitudes of the higher harmonics on the higher side.

6. Concluding remarks

In this work the breathing behaviour of a cracked Jeffcott rotor during passage through critical speed is studied. The response dependent non-linear breathing crack model with partial crack opening that represents the fatigue crack more accurately is shown to yield a higher response, particularly for higher unbalance, than the other approximate models considered in previous studies. The breathing crack model has also helped in understanding the breathing behaviour in finer detail. The effect of various important parameters on breathing behaviour and peak response variation is investigated. The changes in the orbit orientation as the rotor coasts up past the subharmonic resonances is probed and is shown to be a promising method of crack diagnosis. Experimental investigations confirm most of the analytical findings.

The breathing behaviour is shown to depend upon unbalance orientation angle, acceleration rate, crack depth and damping. The breathing behaviour is also different for accelerating and decelerating rotors. For shallow depths and higher damping, the breathing observed at speeds away from the critical speed continues even in the critical speed zone. Thus a linear model instead of the response dependent non-linear model could be used in such cases.

Peak response of the cracked rotor whilst passing through the critical speed depends on unbalance orientation angle, unbalance amount, crack depth, acceleration/deceleration rate and whether the rotor is accelerated or decelerated. For open crack model the peak response during deceleration did not vary much with crack depth.

When unbalance is in phase with the crack ($\beta = 0$), the breathing crack model gives higher response than the switching crack model, whereas when unbalance is in phase opposition ($\beta = 180$), the switching crack model has shown slightly larger response than the breathing crack model. The open crack model shows two maxima (at $\beta = 45^\circ$ and 225°) and two minima (at $\beta = 135^\circ$ and 315°). The breathing and switching crack models gave a single maximum at $\beta = 22.5^\circ$ and a single minimum at $\beta = 157.5^\circ$. The difference between breathing and switching crack model is negligible for very low values of unbalance. However, when the unbalance forces are appreciable the breathing crack model represents the crack more accurately and yields larger response than any other model. Response due to only crack (with negligible unbalance) appears to be maximum at $\beta = 0^\circ$ and minimum at $\beta = 180^\circ$. Addition of unbalance force modifies the response variation for each model. The effect of amount of unbalance is investigated in detail in this study.

At subcritical resonances, both breathing and switching crack models have shown the presence of higher harmonics (3X, 5X) that caused the corresponding subharmonic resonances in the response but the open crack model only showed dominant second harmonic. The orbit orientation changes as the rotor coasts up across various subcritical resonances.

The experimental investigations confirm the typical peak response variation for both the slotted and cracked rotor. In case of a slotted rotor, the peak response for accelerating rotor is found to be less than that for the decelerating rotor for $\beta = 67.5^\circ$ to 135°. The peak response variation is different for low slot depth than for a deeper slot for the same unbalance amount. The amount of

unbalance is clearly seen to affect the peak response variation for a low crack depth ($\bar{a} = 0.23$). The fatigue-cracked rotor has shown response variation similar to the theoretical one. Although the values of β corresponding to minima and maxima of peak response show slight deviation in some cases from analytical investigation, the overall variation is consistently matching with theoretical findings. The typical pattern of response variation with β can be used to distinguish the response of an asymmetric rotor (two maxima and two minima) from that of a cracked rotor (one maxima and one minima). The experimental investigation does make an elaborate comparison between slotted and cracked rotor responses.

A consistent and perceptible change in the orbit orientation during passage through subcritical resonances for the cracked rotor is also observed experimentally. This is proposed to be an additional indicator for diagnosing the presence of crack in rotors. Another important crack indicator, which is analytically observed and experimentally validated is the stronger higher harmonic components in the horizontal direction than in the vertical direction during the passage through subharmonic resonances.

Appendix A. Nomenclature

a	depth of crack
D	diameter of the shaft
$\bar{a}$	crack depth ratio (a/D)
L	length of the shaft
m	mass of the disc
ζ	damping factor
ε	eccentricity of mass of disc from its geometric center
δ_{st}	static deflection of the uncracked rotor
e	dimensionless eccentricity (e/δ_{st})
β	orientation of centre of mass from ξ axis in the direction of shaft rotation
$\theta(t)$	instantaneous angle of rotation of shaft
y, z	rotor center displacement in vertical and horizontal direction respectively
ξ, η	rotor center displacement in the direction perpendicular to crack edge and in the direction parallel to crack edge respectively
k_ξ, k_η	direct stiffness of the shaft in ξ and η directions respectively
$\hat{k}_\xi, \hat{k}_\eta$	stiffnesses in ξ and η directions when the crack is fully open
$k_{\xi\eta}, k_{\eta\xi}$	cross coupled stiffnesses
λ	dimensionless acceleration
ω	rotational speed in rad/s
Ω	dimensionless speed
Ω_{peak}	dimensionless speed at which peak response is attained
τ	dimensionless time
τ_{peak}	dimensionless time at which peak response is attained
g_ξ, g_η	flexibility in ξ and η directions respectively
$g_{\xi\eta}, g_{\eta\xi}$	cross coupled flexibilities
Q_ξ, Q_η	forces acting on the shaft in ξ and η directions respectively

σ_ξ, σ_η stresses acting at a point along the crack edge in ξ and η directions respectively
K^I total stress intensity factor at any point along the crack edge
$K^I_{Q_\xi}, K^I_{Q_\eta}$ stress intensity factor due to forces Q_ξ and Q_η respectively

References

[1] W.B. Wang, Z.S. Duan, X.L. Huang, B.C. Wen, The responses of the simple rotor with surface transverse crack, in: A. Muszynska, J.C. Simonis (Eds.), *Rotating Machinery Dynamics*, DE-Vol. 2, ASME, New York, 1987, pp. 595–600.
[2] D.E. Bently, A.S. Thomson, Detection of cracks in rotors, *Incipient Failure Detection Conference*, Philadelphia, PA, 10–12 March, 1987.
[3] L.R.K. Nilsson, On the vibration behaviour of a cracked rotor, in: *Proceedings of the International Conference on Rotordynamic Problems in Power Plants*, IFToMM, Rome, 1982, pp. 515–524.
[4] A.F.P. Sanderson, The vibration behaviour of a large steam turbine generator during crack propagation through the generator rotor, in: *Vibrations in Rotating Machinery*, Institution of Mechanical Engineers Publications, London, 1992, pp. 263–273.
[5] I.W. Mayes, G.R. Davis, The vibrational behaviour of a multi-shaft, multi-bearing system in the presence of a propagating transverse crack, *Journal of Vibration, Acoustics, Stress, and Reliability in Design* 146 (1984) 146–153.
[6] I.W. Mayes, G.R. Davis, The vibrational behaviour of a rotating shaft system containing a transverse crack, in: *Vibrations in Rotating Machineries*, Institution of Mechanical Engineers Publications, London, 1976, pp. 53–64.
[7] N. Bachschmid, G. Diana, B. Pizzigoni, The influence of unbalance on cracked rotors, in: *Vibrations in Rotating Machinery*, Institution of Mechanical Engineers Publications, London, 1984, pp. 193–198.
[8] B.C. Wen, Y.B. Wang, Theoretical research, calculation and experiments of cracked shaft dynamic response, in: *Vibrations in Rotating Machinery*, Institution of Mechanical Engineers Publications, London, 1988, pp. 473–478.
[9] A. Tamura, Y. Iwata, H. Sato, Unstable vibration of a rotor with a transverse crack, in: *Vibrations in Rotating Machinery*, Institution of Mechanical Engineers Publications, Suffolk, 1988, pp. 647–653.
[10] S. Hisa, H. Sakakida, H. Nakajima, K. Momoeda, T. Noda, Vibration diagnosis for large steam turbine rotor, in: T.S. Sankar, et al. (Eds.), *Diagnostics Vehicle Dynamics and Special Topics*, DE-Vol. 18-5, ASME, New York, 1989, pp. 7–14.
[11] T.A. Henry, B.E. Okah-Avae, Vibrations in cracked shafts, in: *Vibrations in Rotating Machineries*, Institution of Mechanical Engineers Publications, London, 1976, pp. 15–19.
[12] W. Jiang, Z. Luo, Z. Fang, A transient analysis of vertical cracked rotor through critical speed, in: *Proceedings of the International Conference on Hydrodynamic Bearing-Rotor System Dynamics*, X'ian, People's Republic of China, 1990, pp. 278–282.
[13] A.S. Sekhar, B.S. Prabhu, Condition monitoring of cracked rotors through transient response, *Mechanism and Machine Theory* 33 (1998) 1167–1175.
[14] F.H. Kavarana, R.G. Kirk, Crack shaft detection using the unbalance excitation techniques, *ASME Design Engineering Technical Conferences* DE-Vol. 84-2, 1995, pp. 1001–1007.
[15] R.H. Plaut, R.H. Andruet, S. Suherman, Behaviour of a cracked rotating shaft during passage through a critical speed, *Journal of Sound and Vibration* 173 (1994) 577–589.
[16] A.D. Dimarogonas, Vibration of cracked structures: a state of the art review, *Engineering Fracture Mechanics* 55 (1996) 831–857.
[17] N. Bachschmid, A. Vania, S. Audebert, A comparison of different methods for transverse crack modelling in rotor systems, in: *Proceedings of the 8th International Symposium on Transport Phenomenon and Dynamics of Rotating Machinery*, 2000, pp. 1057–1062.
[18] O.S. Jun, H.J. Eun, Y.Y. Earmme, C.W. Lee, Modeling and vibration analysis of a simple rotor with a breathing crack, *Journal of Sound and Vibration* 155 (1992) 273–290.
[19] A. Tondl, *Some Problems of Rotor Dynamics*, Chapman & Hall, London, 1965.

[20] H. Tada, P.C. Paris, G.R. Irwin, *The Stress Analysis of Crack Handbook*, Del Research Corporation, Hellertown, PA, 1973.
[21] C.W. Lee, J.S. Yun, O.S. Jun, Modelling of a simple rotor with a switching crack and its experimental verification, *Journal of Vibration and Acoustics* 114 (1992) 217–225.
[22] H.L. Hassenpflug, R.D. Flack, E.J. Gunter, Influence of acceleration on the critical speed of a Jeffcott rotor, *Journal of Engineering for Power* 103 (1981) 108–113.
[23] R.F. Bosmans, Cracked rotor demonstration, in: *Proceedings of the Symposium on Instability in Rotating Machinery*, NASA Conference Publications 2409 (1985) 443–446.
[24] J. Schmied, E. Kramer, Vibrational behaviour of a rotor with a cross-sectional crack, in: *Vibrations in Rotating Machinery*, Institution of Mechanical Engineers Publications, London, 1984, pp. 183–192.
[25] A. Muszynska, Misalignment and shaft crack-related phase relationships for 1X and 2X vibration components of rotor responses, *Orbit*, September 4–8, 1989.
[26] L.S. Jenkins, Cracked shaft detection on large vertical nuclear reactor coolant pump, *Proceedings of the Symposium on Instability in Rotating Machinery*, NASA Conference Publications 2409 (1985) 443–446.